POLITECNICO DI TORINO

**Master's Degree in Energy and Nuclear Engineering**

**Renewable energy systems**


Master's Degree Thesis

# Mixed Matrix membranes (MMM) based on Carbon-modified Polymers of intrinsic microporosity (PIMs) for Carbon Dioxide (CO2) separation

**Supervisor**

Prof. Sergio Bocchini

**Co-supervisor**

Carmela Astorino

**Candidate**

Laura Cutaia

November, 2023

# Index

# List of Figures

# List of Tables

# 1. Introduction

Rapid industrialization in the past century has led to a surge in energy demand, predominantly met by fossil fuels. This reliance results in significant $CO_2$ emissions, a primary contributor to the greenhouse effect. To address the escalating climate crisis, many countries are exploring strategies like $CO_2$ capture and storage (CCS). Recognized for its potential in aiding climate change targets, CCS offers solutions for low carbon power, industrial decarbonization, and even facilitates net $CO_2$ removal from the atmosphere. [1] [3]

In this research, it was developed and assessed Mixed Matrix Membranes (MMM) infused with Carbon-modified Polymers of Intrinsic Microporosity (PIMs) to enhance $CO_2$ separation efficiency.

The initial part is dedicated to the description of the CCS technologies and the different $CO_2$ separation principles, focusing on Mixed Matrix Membranes that combine the easy processability of polymers and the superior gas separation performance of inorganic materials.

In the chapter 3, related to materials and methods, it is described the synthesis of PIM-1, carboxylated PIM-1 and mesoporous carbons, together with the fabrication of membranes with varying carbon percentages. This requires rigorous testing to determine the best production method.

The subsequent part centers on a discussion about the results obtained from the comprehensive membranes characterization using techniques like Thermo-gravimetric Analysis with IR gas (TGA-IR), FT-IR Spectroscopy (ATR), Differential Scanning Calorimetry (DSC), and Field Emission Scanning Electron Microscopy (FESEM).

In the chapter 5, it is gauged the $CO_2$ absorption capabilities of these materials using a Surface Measurement System equipped with a Dynamic Vapor Sorption (DVS) Instrument. By comparing the permeability, solubility, and diffusivity data across different gases and partial pressures, it is highlighted the enhanced separation performance attributed to carbon incorporation.

The concluding sections focus on enhancing the membrane fabrication procedure and explore potential future perspectives in their utilization.

# 2. $CO_2$ emissions reduction

Rapid industrialization over the past century has resulted in huge demand for energy. The most common source is fossil fuels, but this causes emission of $CO_2$ which is the main component of greenhouse gas (GHG). [1]

According to the International Energy Agency (IEA, 2018), the global mean temperature has been increased by 1 °C above the pre-industrial levels and it is anticipated to reach 1.5 °C by the end of 2040. This increase is associated with climate crisis caused by greenhouse gases emission. [2]

Different approaches are considered and adopted by various countries to reduce their $CO_2$ emissions, including:

- improve energy efficiency and promote energy conservation;
- increase usage of low carbon fuels, including natural gas, hydrogen or nuclear power;
- deploy renewable energy, such as solar, wind, hydropower and bioenergy;
- apply geoengineering approaches (e.g., afforestation and reforestation);
- $CO_2$ capture and storage (CCS). [3]

## *2.1.CCS*

Carbon capture and storage (CCS) is broadly recognised as having the potential to play a key role in meeting climate change targets, delivering low carbon heat and power, decarbonising industry and, more recently, its ability to facilitate the net removal of $CO_2$ from the atmosphere. [4]

The current development progress of different CCS technologies on the TRL scale is shown in in Figure 2.1.

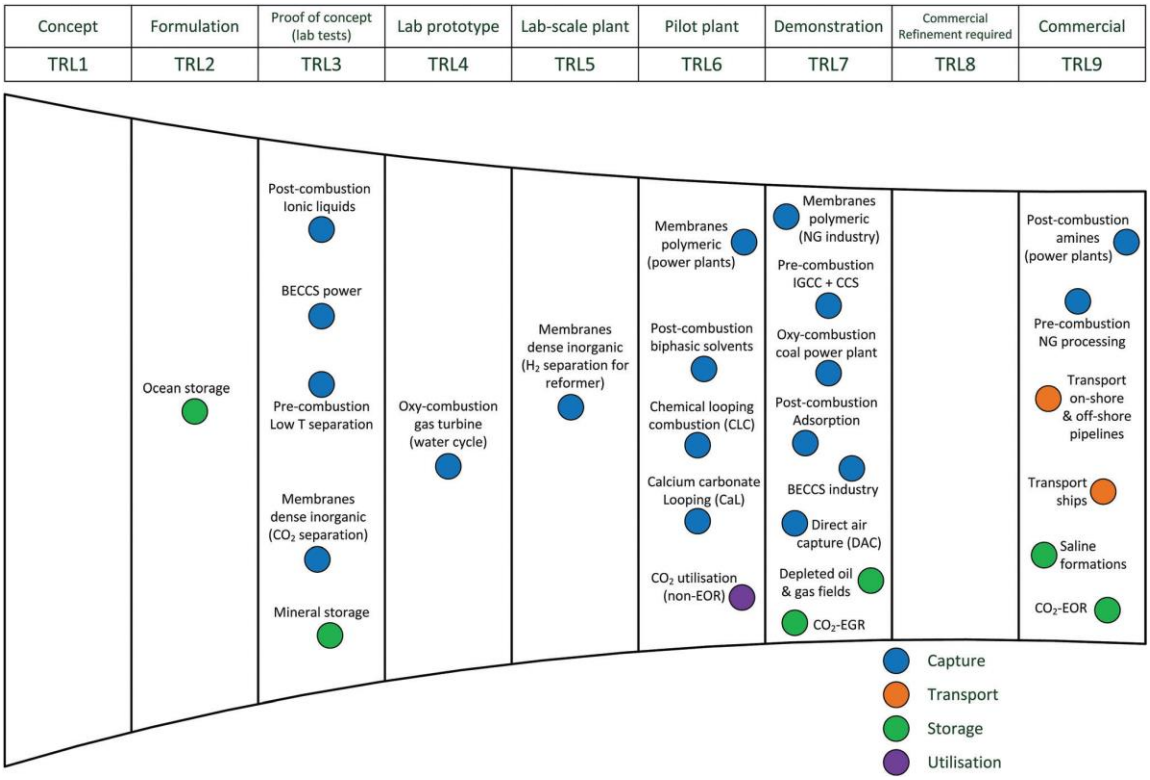


*Figure 2.1: Current development progress of carbon capture, storage and utilization technologies in terms of technology readiness level (TRL).* [4]

The CCS process starts with capturing $CO_2$, followed by transportation of the captured $CO_2$ gas that ends with either utilization or storage. [5]

### 2.1.1. *$CO_2$ capture technologies*

The simplest method of CO2 capture is "carbon capture from point sources." This process involves directly capturing carbon dioxide emissions from specific sources, like power plants or industrial facilities, before they are released into the atmosphere. Specifically for combustion processes there are three main CO2 capture systems associated with post-combustion, pre-combustion and oxyfuel combustion. [3]

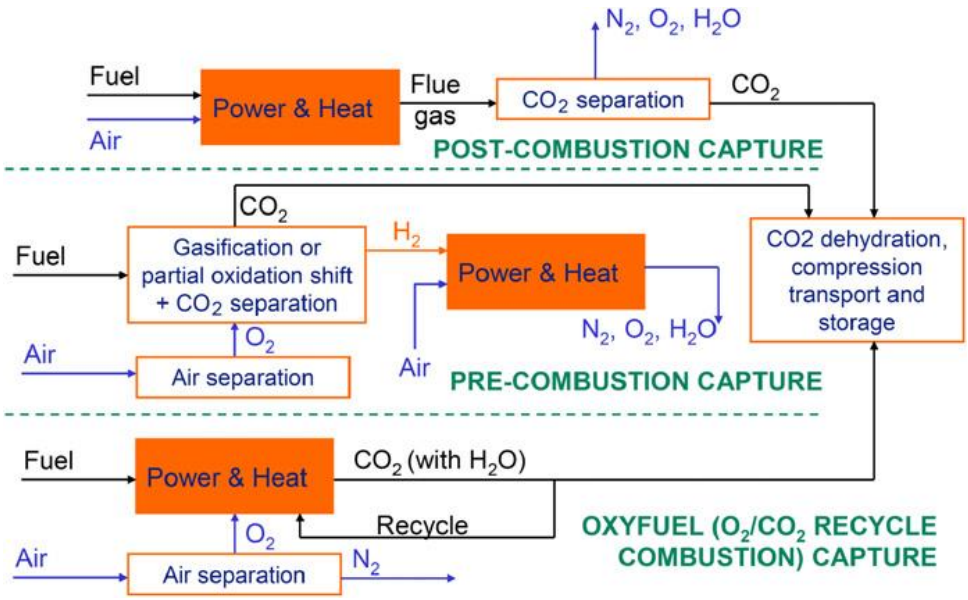


*Figure 2.2: Schematic flow diagram of various $CO_2$ capture technologies.* [6]

1. **Post-combustion**
   In the post-combustion capture process, the $CO_2$ is removed from the flue gas once fossil fuel is burnt followed by storage of the captured $CO_2$. Once the flue gas is burnt to release energy in the form of heat, byproducts such as $CO_2$, water vapor, Sulfur Dioxide ($SO_2$) and Nitrogen Oxides ($NO_x$) are formed. The main process challenges are, the low $CO_2$ concentration in the flue gas, the low $CO_2$ partial pressure that reduces the capture efficiency and increases the energy. Furthermore, the removal of the flue gas pollutants such as $SO_2$ and $NO_x$ increases the energy demand. However, post-combustion represents the best option to be retrofitted to the existing power plants. [5]

2. **Pre-combustion**
   In the pre-combustion capture process, the $CO_2$ is captured before burning the fuel in the combustion chamber. The fossil fuel is reacted with steam and oxygen at elevated temperature and pressure that results in synthesis gas mixture of predominantly CO and $H_2$. Additional water (steam) is then added, and the mixture is passed through a series of catalyst beds for the 'water–gas shift' reaction to approach equilibrium: $CO+H_2O \leftrightarrow CO_2+H_2$. In this way, the CO is converted to $CO_2$ which can be separated to leave a hydrogen-rich fuel gas.
   The separation process typically uses a physical solvent. The pure hydrogen gas is burned to generate electricity. [5] [6]
3. **Oxy-fuel combustion**

The oxy-fuel combustion process is specifically used for coal-fired power plants where pure oxygen (95–99%) is used for burning coal instead of air at high temperature in the combustion chamber. The burning processes produce $CO_2$ that is separated without further processing due to the high $CO_2$ concentration being formed. The $CO_2$ (90% purity) is passed to be compressed and stored. The oxy-fuel combustion carbon capture includes three stages: $O_2$ is separated from air using air separation unit (ASU), pure $O_2$ is used to burn the fossil fuel and energy is generated, and finally the $CO_2$ formed during the burning processes is compressed and transported for storage. The ASU represents the main process challenge due to its high cost. [5]

The advantages and disadvantages of the three technologies are summarized in Figure 2.3. Among them, the post-combustion capture is extensively used and attract the researchers attention. [5]

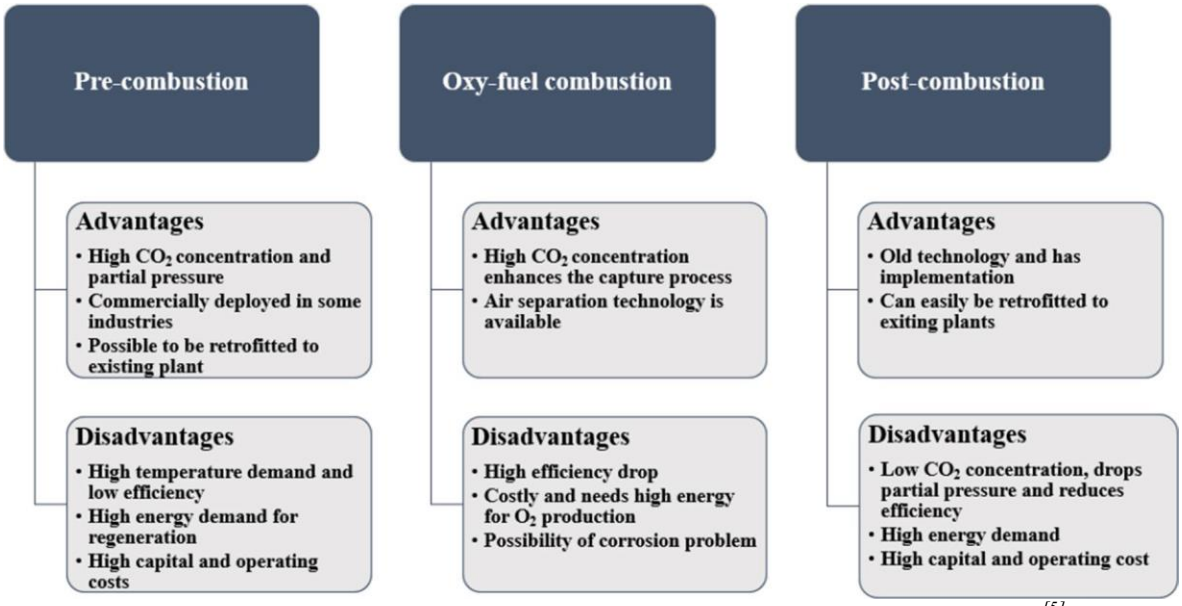


*Figure 2.3: Advantages and disadvantages of the carbon capture technologies.* [5]

### 2.1.2. *$CO_2$ transport*

Once $CO_2$ is separated from the rest of the flue gas components, it needs to be transported to the storage site or to the facilities for its industrial utilization. Whatever the chosen final fate of $CO_2$, a reliable, safe, and economically feasible system of transport is a key feature of any CCS project. Depending on the volumes involved a variety of means of transport may be utilized, ranging from road tankers to ships and pipelines. The last ones represent a viable solution for onshore transport of high volume of $CO_2$ through long distances. Pipelines are also the most efficient way for $CO_2$ transport when the source of $CO_2$ is a power plant which lifetime is longer than 23 years [3]. For shorter period, road and rail tankers are more competitive. For commercial scale CCS projects an extensive network of $CO_2$ pipelines needs to be developed. The pipelines need to be periodically monitored to assess their integrity and an accurate fiscal metering system is to be in place to assure the quantification of the stored fluxes. The equipment used for gas/oil pipelines need to be modified to withstand the challenging environment experienced inside a $CO_2$ pipeline. [3]

### 2.1.3. *$CO_2$ storage*

Geological storage is at present considered to be the most viable option for the storage of the large $CO_2$ quantities needed to effectively reduce global warming and related climate change. Three different geological formations are commonly considered for $CO_2$ storage: depleted (or nearly depleted) oil and gas reservoirs, unmineable coal beds and saline aquifers. Deep ocean storage is also a feasible storage option although environmental concerns, such as ocean acidification and eutrophication, will likely limit its application. A typical geological storage site can hold several tens of million tonnes of $CO_2$ trapped by different physical and chemical mechanisms. General requirements for geological storage of $CO_2$ include appropriate porosity, thickness, and permeability of the reservoir rock, a cap rock with good sealing capability, and a stable geological environment. Requirements such as distance from the source of $CO_2$, effective storage capacity, pathways for potential leakage and in general economic constrains may limit the feasibility of being a storage site. [3]

### 2.1.4. *$CO_2$ utilization*

There are numerous options to utilize $CO_2$ after the carbon capture process as shown in Figure 2.4. The captured $CO_2$ can be used to produce chemicals and fuels, as solvents and to convert solar energy into chemical energy via artificial photosynthesis. Furthermore, $CO_2$ can be utilized for enhanced oil recovery (EOR) and enhanced coal bed methane (ECBM) recovery. These technologies are well developed than the others; however, these processes can be made more efficient. Most of the $CO_2$ utilization techniques are still in the development phase and require more analysis and resources to make them financially viable. For the feasibility assessment, the $CO_2$ utilization technique should be analysed with respect to energy, economics and environmental. [7]

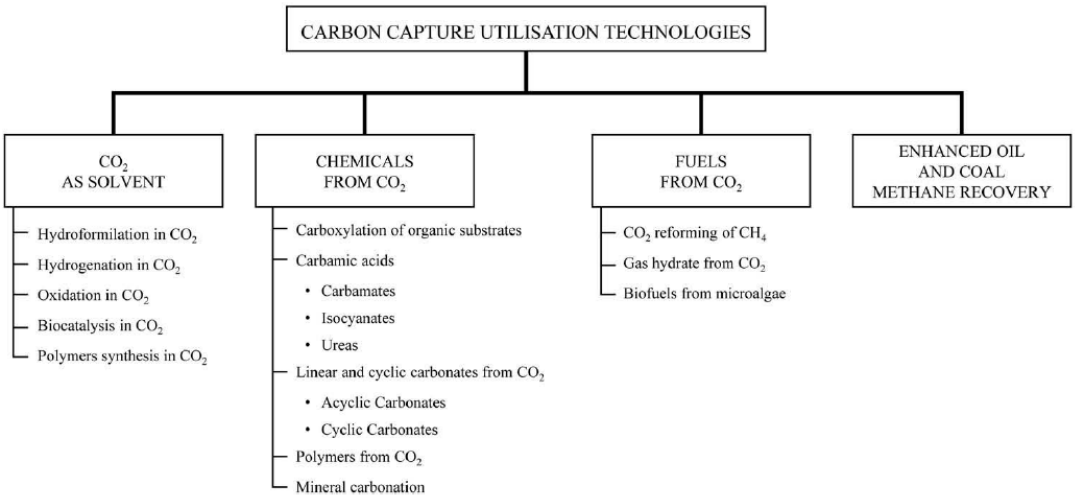


*Figure 2.4: $CO_2$ utilization technologies.* [7]

## *2.2. Carbon dioxide separation principles*

### 2.2.1. *Absorption*

Absorption processes are widely used in the petroleum, natural gas and coal fired power plants as well as chemical industries for separation of $CO_2$ from the flue gas thanks to the use of a liquid sorbent. [3] [8]

In this method absorber and regenerator are working continuously. Flue gas stream containing $CO_2$ is introduced at the bottom of the absorber. Absorbent is introduced from top of the column that leads counter current contact between flue gas and solvent and a selective absorption of $CO_2$ takes place. Then $CO_2$ rich stream is fed to the regenerator, where desorption of $CO_2$ occurs and regenerated solvent is recycled for further use, desorbed $CO_2$ is compressed and sent to storage. [8]

Typical sorbents include monoethanolamine (MEA), diethanolamine (DEA) and potassium carbonate. Some other sorbents, such as piperazine and anion-functionalized ionic liquid have also received attention in recent years. Piperazine has been found to react much faster than MEA, but because it has a larger volatility than MEA, its application in $CO_2$ absorption is more expensive and is still under development. One important challenge for the large deployment of this technology for CCS is its potential amine degradation, resulting in solvent loss, equipment corrosion and generation of volatile degradation compounds. Moreover, amine emissions can degrade into nitrosamines and nitramines, which are potentially harmful to the human health and the environment. [3]

### 2.2.2. *Adsorption*

Adsorption is a process for removal of one or more components of a mixture with the help of a solid surface. The adsorption processes are based on significant intermolecular forces between gases (including $CO_2$) and the surfaces of certain solid materials, such as molecular sieves, activated carbon, zeolites, calcium oxides, hydrotalcites and lithium zirconate. Depending on the temperature, partial pressure, surface force and adsorbent pore sizes, single or multiple layers of gases can be adsorbed. In $CO_2$ capture by adsorption technology, a packed column is mainly filled by spherical adsorbent and $CO_2$ bearing stream is passed through the column. $CO_2$ is attracted towards the adsorbent and adheres on the surface of adsorbent. After achieving the equilibrium, desorption takes place to get $CO_2$ in pure form and regenerated adsorbent can be utilized for further cycle. The adsorbed $CO_2$ can be recovered by swinging the pressure (PSA) or temperature (TSA) of the system containing the $CO_2$-saturated sorbent. PSA is a commercially available technology for $CO_2$ recovery from power plants that can have efficiency higher than 85%. In this process, $CO_2$ is preferentially adsorbed on the surface of a solid adsorbent at high pressure, which will swing to low pressure (usually atmospheric pressure) to desorb the adsorbent and release $CO_2$ for subsequent transport. In TSA, the adsorbed $CO_2$ will be released by increasing the system temperature using hot air or steam injection. The regeneration time is normally longer than PSA but $CO_2$ purity higher than 95% and recovery higher than 80% can be achieved. Finally, the use of residues from industrial and agricultural operations to develop sorbents for $CO_2$ capture has attracted significant attention to reduce the total costs of capture. [3] [8]

### 2.2.3. *Cryogenic distillation*

Cryogenic distillation is a gas separation process using distillation at very low temperature and high pressure. Differently from other conventional distillation processes, it is used to separate components of gaseous mixture (due to their different boiling points) instead of liquid. For $CO_2$ separation, flue gas containing $CO_2$ is cooled to desublimation temperature and then solidified $CO_2$ is separated from other light gases and compressed to a high pressure of 100–200 atmospheric pressure. The amount of $CO_2$ recovered can reach 90–95% of the flue gas. Since the distillation is conducted at extremely low temperature and high pressure, it is an energy intensive process. Several patented processes have been developed and research has mainly focused on cost optimization. [3]

### 2.2.4. *Chemical looping combustion*

A metal oxide is used as an oxygen carrier instead of using pure oxygen directly for the combustion as in the case of oxyfuel combustion. During the process the metal oxide is reduced to metal while the fuel is being oxidized to $CO_2$ and water. The metal is then oxidized in another stage and recycled in the process. Water, the process by-product, can be easily removed by condensation, while pure $CO_2$ can be obtained without consumption of energy for separation. There are a wide variety of metal oxides that are of low-cost and suitable for this process including $Fe_2O_3$, NiO, CuO and $Mn_2O_3$. [3]

### 2.2.5. *Hydrate-based separation*

Hydrate-based $CO_2$ separation is a new technology by which the exhaust gas containing $CO_2$ is exposed to water under high pressure forming hydrates. The $CO_2$ in the exhaust gas is selectively engaged in the cages of hydrate and is separated from other gases. The mechanism is based on the differences of phase equilibrium of $CO_2$ with other gases, where $CO_2$ can form hydrates easier than other gases such as $N_2$. This technology has the advantage of small energy penalty. [3]

### 2.2.6. *Membrane separation*

A relatively novel capture concept is the use of selective membranes to separate certain components from a gas stream, which can be $CO_2$ from flue gas (post-combustion system), $CO_2$ from natural gas and $CO_2$ from hydrogen (pre-combustion systems) or oxygen from nitrogen (in oxyfuel combustion system). Membranes are semi-permeable barriers able to separate substances by various mechanisms: solution/diffusion, adsorption/diffusion, molecular sieve and ionic transport. They are available in different material types, which can be either organic (polymeric) or inorganic (carbon, zeolite, ceramic or metallic) and can be porous to non-porous. Membranes act as filters to separate one or more gases from a feed mixture and generate a specific gas rich permeate as shown in Figure 2.5, below. [9]

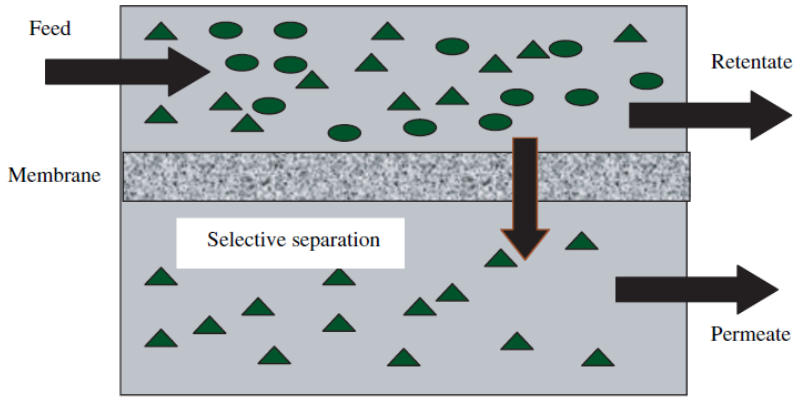


*Figure 2.5: Schematic of gas-separation membrane.* [3]

The choice of a membrane material for gas separation applications is based on specific physical and chemical properties since these materials should be tailored in an advanced way to separate particular gas mixtures. Moreover, robust (i.e., long-term and stable) materials are required to be applied in a membrane gas separation process.

The gas separation properties of membranes depend upon:

• the material (permeability, separation factors),

• the membrane structure and thickness (permeance),

• the membrane configuration (e.g., flat, hollow fiber),

• the module and system design.

The two characteristics that dictate membrane performance and influence the economics of the gas separation process are: permeability and selectivity. The first one is the rate at which any compound permeates through a membrane. The second one is the membrane's preference to pass one gas species over the other. Selectivity is a key parameter to achieve high product purity at high recoveries. Membranes have several advantages over absorption and adsorption processes such as no regeneration energy required, simple modular systems and no waste streams but they cannot always achieve high degrees of separation, which makes multiple stages or recycling necessary. Membrane gas separation has the potential to grow enormously if more selective membranes will become available. [9] [10]

## *2.3.Membrane and gas permeation parameters*

In polymer-based membranes, the gas transport phenomenon can be described through some fundamental parameters to evaluate the membrane material performance.

The gas **permeability coefficient, $P_A$**, of a pure gas permeating through a polymer membrane is typically expressed in Barrer where:

$$1\ Barrer = \frac{10^{-10}\ \ cm^3(STP)\ cm}{cm^2\ \ s\ cmHg}$$

Using the solution-diffusion model, $P_A$ can be written as the product of a gas solubility coefficient, $S_A$, and a concentration-averaged, effective diffusion coefficient, $D_A$:

$$P_A = D_A \cdot S_A \tag{2.1}$$

In the Barrer formula the diffusion coefficient is expressed in $cm^2$/sec, and solubility is expressed in $cm^3$(STP)/($cm^3$ polymer atm) or $cm^3$(STP)/($cm^3$ polymer cmHg).

Each polymer has a different permeability coefficient for each gas, and the faster permeation of some gases relative to others provides the basis for the use of polymers to separation gas mixtures.

Diffusion coefficients are also sensitive to polymer chain flexibility and the free volume in the polymer, which depends on the amount of packing defects, gaps between polymer chains and other structural features that give rise to openings within a polymer large enough to permit penetrant diffusion. Free volume is among the most important structural variables influencing gas transport properties in polymers. The Cohene Turnbull model predicts that diffusion coefficients increase strongly as free volume increases.

The **solubility coefficient, $S_A$,** is defined as the ratio of the concentration of gas in a polymer, $C$, to the pressure of gas, $p$, contiguous to the polymer:

$$S_A = \frac{C}{p} \tag{2.2}$$

Solubility depends mainly on gas molecule condensability and, to a lesser extent, on gas-polymer interactions. Polymer morphological features, such as crystallinity and liquid crystallinity, also influence gas solubility in polymers.

The **ideal selectivity, $\alpha_{A/B}$**, often treated as a material property of a polymer, characterizes the ability of a polymer to separate two gases (e.g., A and B) and it is defined as:

$$\alpha_{A/B} = \frac{S_A}{S_B} \tag{2.3}$$

By combining the equations (2.1) and (2.3), permeability selectivity can be written as a product of solubility and diffusivity selectivity [11]:

$$\alpha_{A/B} = \frac{D_A}{D_B}\frac{S_A}{S_B} \tag{2.4}$$

Polymeric membranes generally undergo a trade-off limitation between permeability and selectivity: as selectivity increases, permeability decreases, and vice versa. Robeson, collecting a large number of permeation data for different polymeric membranes, showed as for small gaseous molecules (e.g., $O_2$, $N_2$, $CO_2$, and $CH_4$) a superior limit (upper bound) exists in a selectivity/permeability diagram. The upper bound would represent the asymptotic end point in the performance of polymeric membranes whose separation properties are related to solution-diffusion transport mechanisms. [10]

Comparing the chemical and physical properties of different gases, shown in Table 2.1, it is possible to observe that $CO_2$ presents higher condensability than all other gases (higher critical temperature) and a smaller kinetic diameter than $N_2$ and $CH_4$, which results in easier mobility and accessibility in the free volume of the membrane. [12]

| **Gas** | **Kinetic diameter ($\dot{A}$)** | **$T_{critical}$ ($°C$)** |
|---|---|---|
| $H_2$ | 2.89 | -229.91 |
| $CO_2$ | 3.30 | 31 |
| $N_2$ | 3.64 | -147.1 |
| $CH_4$ | 3.80 | -82.62 |

*Table 2.1: Chemical and physical properties of gases.* [12] [25]

## *2.4. Carbons for gas separation*

There is an urgent need to reduce the $CO_2$ level by capture at the point sources of emissions. [22]

Technologies based on absorption are currently the most mature and industrialized, by using liquid amines that chemically interact with the $CO_2$ molecules. However, several limitations have still to be solved, such as severe corrosion of the equipment and high energy consumption for absorbent regeneration. To overcome these issues, adsorption technology benefits lower operation costs and adsorbent reusability compared with the other technologies.

Solid-sorbent families such as zeolites, metal-organic frameworks, porous silicas, porous polymers, and porous carbons are the most used to capture $CO_2$, mainly via physical adsorption. Among them, porous carbons are advantageous because they can be obtained with large surface area, tunable porous structure, and surface properties. At the same time, they have good thermal and chemical stability and resistance to moisture. Their cost-effectiveness is related to the production process; commercial and cheap highly porous carbons are also available and used commercially, for instance, the ones derived from low-cost biomass feedstock. A critical aspect of physical adsorbents is the low selectivity for $CO_2$ in a mixture with other gases, as typically occurs in flue gases.

The design of the pore architecture and the adjustment of the surface properties are the most used strategies for promoting a selective adsorbate-adsorbent interaction. It is generally agreed that micropores (<2 nm) and ultramicropores (<0.7 nm) are crucial for boosting both $CO_2$ adsorption and selectivity because of the higher adsorption potential in very small pores. However, in the microporous network, the $CO_2$ diffusion is affected by slow kinetics and inaccessibility. An ordered porous architecture composed by combining micropores and mesopores improves the $CO_2$ uptake. Indeed, despite templated synthetic routes increase the overall cost of the process, by involving expensive chemicals and multiple time-consuming reaction steps, ordered mesoporous carbons (OMCs) are still competitive from an application point of view. The ordered porous network facilitates gas transport and makes the adsorption sites available to the adsorbate.

The heteroatom incorporation onto the carbon surface is a widely explored strategy for enhancing the interaction with $CO_2$. Specific functionalization with N-based moieties is widely used for increasing the basicity of the carbon framework, thus promoting the interaction with the acidic $CO_2$ molecule. However, microporosity and nitrogen doping are frequently obtained via post-synthesis processes, such as physical or chemical activation and treatments with ammonia and/or functionalization with amine groups, respectively. Additional stages in the adsorbents preparation procedure increase time/energy consumptions, which in turn increase the overall cost and impact over industrial up-scaling. [23]

## *2.5.Mixed Matrix Membrane (MMM)*

Mixed-matrix membranes (MMMs) represent a recognized approach for improving the characteristics of polymeric membranes. Their microstructure consists of an inorganic material in the form of micro- or nanoparticles (discrete phase) incorporated into a polymeric matrix (continuous phase), as shown in Figure 2.6. [13]

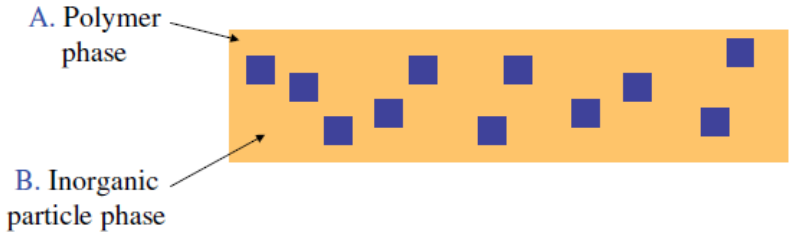


*Figure 2.6: Schematic of a mixed matrix membrane (MMM).* [13]

The successful development of MMMs depends on several factors, such as the proper selection of polymeric matrix and inorganic filler and the elimination of interfacial defects between the two phases. It is also important to control filler concentration, shape, and dimensions in order to reach the expected performance. Several inorganic materials, porous and nonporous, were considered for the preparation of MMMs. These inorganic particles can improve the separation (e.g., by molecular sieving mechanism) or increase the membrane free volume. The use of two materials with different flux and selectivity provides the possibility to better design a gas separation membrane, allowing the synergistic combination of polymers' easy processability and the superior gas separation performance of inorganic materials. In principle, the incorporation of the inorganic component can be seen as a relatively easy modification of existing methods for fabricating large-surface area polymeric membranes; therefore, MMMs possess an economic advantage over inorganic membranes. In addition, they may offer enhanced physical, thermal, and mechanical properties for aggressive environments and could be a way to stabilize the polymer membrane against change in permselectivity with temperature. These membranes offer very interesting properties; however, their cost, difficulties for commercial scale manufacture, and brittleness remain important challenges. [10]

## *2.6.PIM-1*

Polymers of intrinsic microporosity, PIMs, are a novel microporous material attracting attention due to their potentially useful functional properties. [26]

Intrinsic microporosity in polymers is defined as "a continuous network of interconnected intermolecular voids, which forms as a direct consequence of the shape and rigidity of the component macromolecules". In general, polymers pack space so as to maximize attractive interactions between the constituent macromolecules and, hence, minimize the amount of void space. Most polymers have sufficient conformational flexibility to allow them to rearrange their shape to maximize intermolecular cohesive interactions and pack space efficiently. On the contrary, in case of PIMs, the approach to maximizing intrinsic microporosity is that to design polymers with highly rigid and contorted molecular structures to provide "awkward" macromolecular shapes that cannot pack space efficiently. [27]

The distinct macromolecular structure of polymers of intrinsic microporosity, PIMs, provides organic materials with a unique combination of properties including good solubility, exceptional chain rigidity, and high free volume, which support the rapid and selective transport of small molecules. PIMs are directly solution-processable into useful forms such as membranes that can act as efficient molecular sieves. The first PIMs were reported in 2004 by Budd and McKeown. [15]

The intrinsic microporosity property of PIMs, coupled with their solution processability and selectivity in transferring molecular moieties make them of great interest in various applications including [26]:

- catalysis,
- liquid phase separations (such as wastewater purification),
- membrane gas separation,
- organic vapour sensing,
- hydrogen storage. [26]

The most well-studied linear microporous polymer is the polymer of intrinsic microporosity 1, PIM-1, shown in Figure 2.7. [15] [16] [17]

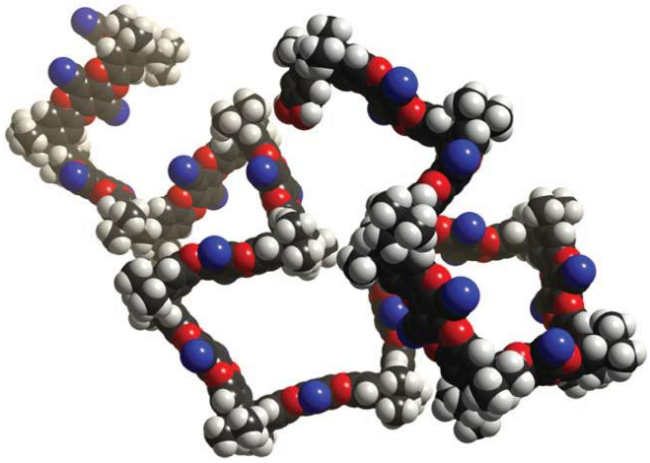

*Figure 2.7: A molecular model of a small fragment of PIM-1 showing its rigid and contorted structure.* [17]

It has a characteristic spirocenter between cyclopentane rings that hinders efficient chain packing. These 90° bends in the polymer chain impart “intrinsic” microporosity (pore size < 2 nm, as defined by IUPAC) and high free volume. [16]

PIMs, and specifically PIM-1, have shown a promising combination of permeability coefficient and permselectivity. [18]

They also often exhibit gas transport behavior near or above the Robeson upper bound, which is a common benchmark used to compare polymer performance and explain the trade-offs in permeability and selectivity. [14]

## *2.7.cPIM-1*

The carboxylated PIM-1, cPIM-1, is obtained by a chemical modification to replace nitrile groups (−CN) by carboxylic groups (−COOH) through hydrolysis. [19]

After incorporating the carboxylic acid group, permeation significantly decreases when compared to PIM-1, while the selectivity increases by >100% for $CO_2/N_2$, $CO_2/CH_4$, $O_2/N_2$, and $H_2/N_2$ gas pairs. In general, cPIM-1 displays a more prominent size-sieving or diffusion-selective mechanism of transport than PIM-1, especially for gas pairs with significantly different kinetic diameters (i.e., $CO_2$ and $CH_4$).

It is interesting to analyze the behavior of PIM-COOH under more realistic conditions and to evaluate the effect of hydrogen bonding on $CO_2$ exposure by performing high-pressure $CO_2$ permeation tests on PIM-1 and PIM-COOH films.

The results show that in a pure-gas scenario, the plasticization pressure point of PIM-1 (15 atm) is higher than that of PIM-COOH (5 atm).

Plasticization is a phenomenon where highly polarizable gases, such as $CO_2$, at high enough concentration, can induce chain mobility in polymers and lead to a reduction in permselectivity in mixed-gas scenarios.

In the case of PIM-COOH, these findings may indicate a disruption of secondary interactions when exposed to $CO_2$. From this interpretation, as pressure increases and the $CO_2$ concentration rises, hydrogen bonding between −COOH groups on the polymer backbone may be disrupted, leading to increased free volume and thus, higher $CO_2$ diffusion at high pressures.

However, despite the plasticization effects, PIM-COOH exhibits excellent mixed-gas transport performance on the 2018 mixed-gas upper bound. [14]

## *2.8.Mesoporous carbons utilized*

Selective and high-performing ordered mesoporous $CO_2$ adsorbents, with remarkable features of sustainability and regenerability, were prepared thanks to the use of D-glucosamine hydrochloride, which is obtained from the hydrolysis of chitin, the second most abundant natural polysaccharide.

D-glucosamine hydrochloride was successfully explored as a sustainable carbon/nitrogen, C/N, precursor for the synthesis of nitrogen-containing ordered mesoporous carbons, NOMCs, obtained through the nanocasting technique and specifically conceived for selective $CO_2$ adsorption. [23]

The nanocasting pathway is closely related to the casting process on the macroscopic scale: a rigid mold with voids in the desired shape (morphology, surface curvature) is first filled with materials or precursors. During processing, the materials are solidified and a negative replica which replicates the void structure can be obtained after removing the mold. Thus, the fabrication of the mold plays an important role in the nanocating pathway. [24]

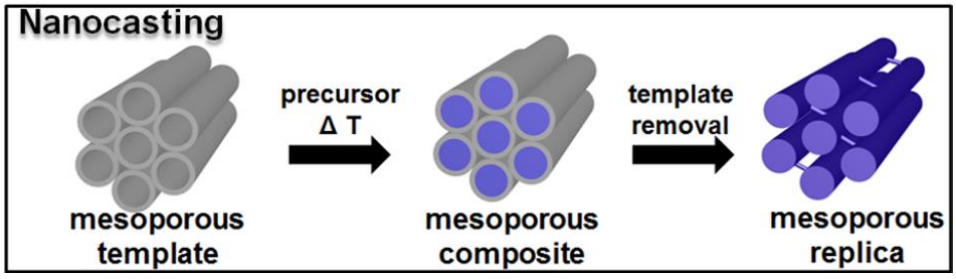


*Figure 2.8: Schematic illustration for the nanocasting using ordered mesoporous materials as the hard template.* [24]

The novel NOMC materials are prepared by impregnating D-glucosamine into the pores of the KIT-6 ordered mesoporous silica hard-templates followed by pyrolysis and silica removal steps. [23]

The pyrolysis temperature affects the development of microporosity. The lower pyrolysis temperature (600 °C) allows for the retention of a higher amount of N inclusions in the carbon framework, mainly in the form of pyrrolic-N and pyridinic-N, the latter being particularly beneficial for improving the selective adsorption of $CO_2$. [23]

So, proper combination of the suitable C/N precursors, the synthesis conditions, and the pore architecture are highly effective in obtaining high performing, sustainable, and reusable $CO_2$ sorbents, without any need for time/energy consuming activation steps or N-doping post-treatments. [23]

# 3. Materials and methods

## *3.1.Material*

2,3,5,6-Tetrafluoroterephtalonitrile (TFTPN) was purchased by Fluoro Chem.

3,3,3,3'-Tetramethyl-1,1'-spirobiindane-5,5',6,6'-tetraol (TTSBI), Dichloro-p-xylene, Benzimidazole, Potassium carbonate ($K_2CO_3$) and all solvent were purchased from Merk-Sigma-Aldrich.

## *3.2.Methods*

### 3.2.1. *Synthesis of PIM-1*

PIM-1 was synthesized following a previously reported method. [20]

The reactants, 3,3,3',3'- Tetramethyl-1,1-spirobiindane- 5,5,6,6-tetraol (9 g) and 2,3,5,6-Tetrafluoroterephthalonitrile (5.2 g), were solubilized in separate vials at a temperature of 40 °C. They were equipped with rubber septa to perform nitrogen vacuum cycles using needles to maintain a deoxygenated environment that could affect the subsequent polymerization step. In a three-necked flask equipped with a magnetic anchor, potassium carbonate, $K_2CO_3$ (16.6 g), was introduced, which serves to neutralize the hydrofluoric acid produced as a byproduct of the reaction, along with an aliquot of Dimethylformamide, DMF, (180 ml). The reflux condenser was set up, and the other openings were sealed with rubber septa. Nitrogen was introduced through a needle to remove any traces of oxygen. A temperature of 65°C was set using an oil bath. The reagents were introduced with a syringe and stirred magnetically to allow the reaction to proceed for 72 h.

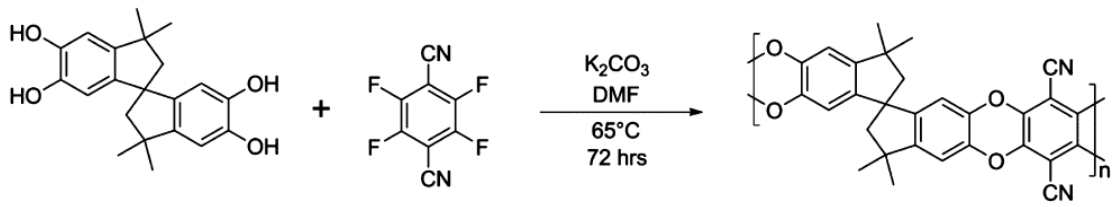


*Figure 3.1: Synthesis of PIM-1.* [16]

After 72 h, the reaction was stopped by precipitation in water (400 ml) and stirred for 15 min, after which the suspension was filtered under vacuum conditions using a filtration system. The solid was re-dispersed in deionized water to repeat the washing process three times, ensuring both the removal of the solvent and the solubilization of the unreacted bicarbonate. The same procedure was carried out with a solvent change, such as methanol, to eliminate both water and any unreacted reagents, as well as to have a solvent with a lower boiling point. In fact, the wet solid was transferred to a beaker and then moved to a vacuum oven at 40 °C overnight to be dried.

The resulting yellow powder was then transferred to a calibrated vial and placed in a vacuum system (Buchi) at 100 °C overnight to remove any traces of water or residual DMF. At the end of the synthesis, the compound appears as a much finer powder [20], as shown in Figure 3.2.

*Figure 3.2: Powder of PIM-1.*

### 3.2.2. *Synthesis of cPIM-1*

The cPIM-1 was synthesized modifying a previously reported method. [19]

PIM-1 was hydrolyzed into cPIM-1. Hydrolysis is the reaction involving the transformation of nitrile group (−CN) into carboxylic group (−COOH). PIM-1 powders (2 g) were first dispersed in a solution (40 ml) of sodium hydroxide (NaOH, 20 wt%) in ethanol and water mixture with a 1:1 ratio in weight. The mixture was then placed in the microwave reactor, equipped with a magnetic stirrer to ensure mixing, and the reaction was conducted for 1 h at 120 °C.

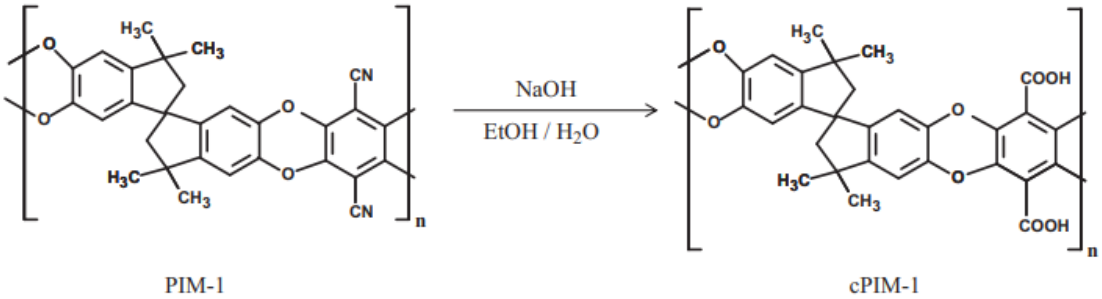


*Figure 3.3: Synthesis of cPIM-1.* [19]

At the end of the reaction, the obtained gel was precipitated in deionized water by adding 37% concentrated hydrochloric acid, HCl, reducing the pH to around 4-5 from the previously strongly basic solution, and left under agitation overnight. The polymer precipitates, and two phases, liquid solid, can be distinguished, with sodium chloride, NaCl, solubilized in the liquid phase as a byproduct of acidification.

Once confirmed an acidic pH the content was filtered to recover the polymer (Nylon filter, D=47 mm, mesh 0.22 μm) by performing washing cycles first in water and then methanol (three cycles). Before proceeding with the methanol washing cycles, it was also ensured that the pH was neutral, around 7. The filtered product appears as a pasty solid, which was transferred to a vacuum oven (gradually heated to 40°C) and then to a vacuum system (Buchi) at T=100°C.

*Figure 3.4: Powder of cPIM-1.*

### 3.2.3. *Synthesis of Mesoporous Carbons*

Carbons were provided by Mirtha Lourenço from The University of Aveiro, and they were produced according to the protocol described as follows.

N-doped biochar was prepared through the pyrolysis of the commercial chitosan (medium molecular weight, degree of deacetylation of 75 - 85%, and low viscosity (200 - 800 cps for 1% acetic acid) from Sigma Aldrich) under $N_2$ flux at 600 °C employing microwave-assisted heating. Typically, 1.5 g of chitosan commercial powder was weighted in the crucible and placed inside the Phoenix™ Microwave Muffle Furnace. Under a $N_2$ flow, the pyrolysis was performed following the heating procedure: i) 5 °C/min, 200 °C, 5 min and ii) 5 °C/min, 600 °C, 20 min to afford CTOP600_MW with a 31.6 % yield.

### 3.2.4. *cPIM-1 based membrane preparation procedure*

Firstly, solubility tests of cPIM-1 were carried out using ten types of solvents using about 25 mg of cPIM-1 and 0.5 ml of solvent.

The membrane preparation process, based on solvent casting, involved hot solubilization of cPIM-1 in the solvent in a silicone bath heated at a temperature of 100 °C. The optimized quantities involved for the realization of one membrane are: 200 mg of cPIM-1 and 3 ml of solvent. The solution obtained was poured on a proper support placed on a heated plate to promote the evaporation of the solvent and subsequently transferred to a vacuum oven at 40 °C to be dried. After making the die-cuts (weight needed about 20 mg), they and the membrane were put to a vacuum system (Buchi) at T=100°C.

With the purpose of selecting the best solution, several tests were carried out to make membranes of cPIM-1 using supports of different materials, such as glass petri, nylon, polytetrafluoroethylene (PTFE) and low-density polyethylene (LDPE). Specifically, for each type of support, three membranes of cPIM-1 solubilized in DMF, DMSO and NMP, respectively, were obtained. The plate was heated to a temperature range between 60 °C and 125 °C, according to the solvent used. The details of each test are reported in the Appendix. Once the best solvent was identified, it was applied for the realization of all membranes.

### 3.2.5. *cPIM-1 with carbons-based membrane preparation procedure*

Once the optimal support and solvent for cPIM-1 membranes were identified, the same procedure was applied for the realization of cPIM-1 with carbons-based membrane. The only step that changes is that related to solubilization, in fact the membrane was prepared by weighing cPIM-1 and carbons into two separate vials, which were then solubilized and dispersed in a specific quantity of solvent. The quantities involved are the following:

| **Membrane** | **cPIM-1 (mg)** | **Solvent (ml)** | **Carbons (mg)** |
|---|---|---|---|
| 5% w/w | 160 | 2.4 | 8.4 |
| 2% w/w | 160 | 2.4 | 3.3 |
| 1% w/w | 160 | 2.4 | 1.6 |

*Table 3.1: cPIM-1 with carbons-based membrane quantities.*

The solution was poured on the support placed on a heated plate at 60 °C, and subsequently transferred to a vacuum oven at 40 °C. After making the die-cuts, they and the membrane were put to a vacuum system (Buchi) at T=100°C.

### 3.2.6. *Density*

Density was evaluated by die-cut some specimens, with a diameter equal to 1 cm each. Five cylinders were obtained. Of these, the mass (mg) and thickness (μm) were measured and then the volume was calculated as: $volume = surface\ area \cdot thickness$.

## *3.3. Instrumental methods*

### 3.3.1. *FT-IR spectroscopy*

Infrared spectra were obtained for each sample using the Bruker Invenio spectrometer, which was equipped with a DTGS (deuterated triglycine sulfate) detector, and a Bruker Platinum attenuated total reflectance (ATR) accessory featuring a diamond crystal. The acquisition of infrared spectra involved recording 24 scans at a resolution of 4 $cm^{-1}$ within the spectral range of 4000 to 400 $cm^{-1}$ for both the background and the sample.

### 3.3.2. *Thermo-gravimetric analysis coupled with IR gas analysis (TGA-IR)*

Thermo-gravimetric measurements and infrared gas analysis were performed. Thermo-gravimetric measurements were conducted using a Netzsch TG 209 F1 Libra instrument. Approximately 5 mg of the sample was heated from 30°C to 800°C at a rate of 10°C/min while exposed to a nitrogen flow of 40 ml $min^{-1}$. The gases evolved during the process were analyzed using a Bruker infrared spectrophotometer, which was coupled with a heated transfer line.

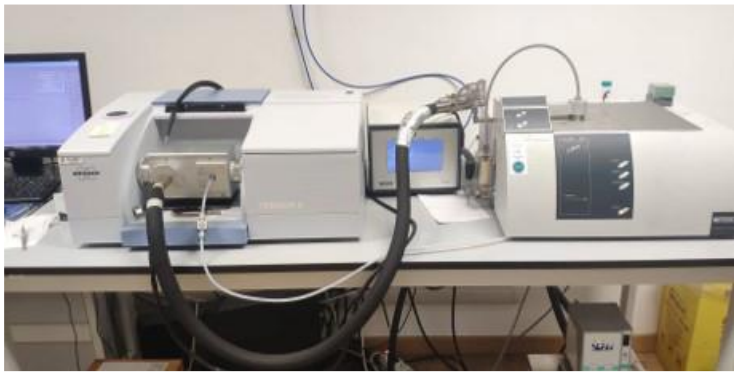

*Figure 3.5: TGA-IR instrumental setup. On the right: TGA instrument; on the left: IR spectrometer equipped with gas phase transmission accessory; in the middle: heated transfer line and temperature controller.*

### 3.3.3. *Differential scanning calorimetry (DSC)*

The thermal stability of the membranes was evaluated through differential scanning calorimetry (DSC) analysis using a Netzsch DSC 204 F1 Phoenix instrument. Heat flux measurements were recorded during both heating and cooling cycles over a temperature range spanning from -65°C to 150°C, with a heating and cooling rate of 10°C/min. The data acquired during these experiments were subsequently analyzed and processed using the Netzsch Proteus Analysis software.


*Figure 3.6: DSC instrument.*

### 3.3.4. *Field Emission Scanning Electron Microscopy (FESEM)*

Field emission scanning electron microscopy (FE-SEM,Zeis SupraTM 25 (Oberkochen, Germany)) was employed to examine both the surface morphology and thickness of the manufactured membranes. Before conducting the analysis, the membranes underwent brittle fracture by exposure to liquid nitrogen.


*Figure 3.7: FESEM instrument.*

## *3.4.Instrumental methods for assessing $CO_2$ uptake*

### 3.4.1. *Microbalance*

The assessment of materials' $CO_2$ absorption capability was conducted using a Surface Measurement System equipped with a Dynamic Vapor Sorption (DVS) Instrument. The procedure involved subjecting a membrane to a sequence of adsorption and desorption cycles with $CO_2$ gas. The weight change of the membrane was continuously monitored. These cycles encompassed a spectrum of gas partial pressures ranging from 0% to 80% for $CO_2$, hydrogen ($H_2$), methane ($CH_4$) and nitrogen ($N_2$). The highest attainable $CO_2$ absorption capacity was determined at each specific partial pressure level. It's noteworthy that all experiments were carried out at a temperature of 40°C.

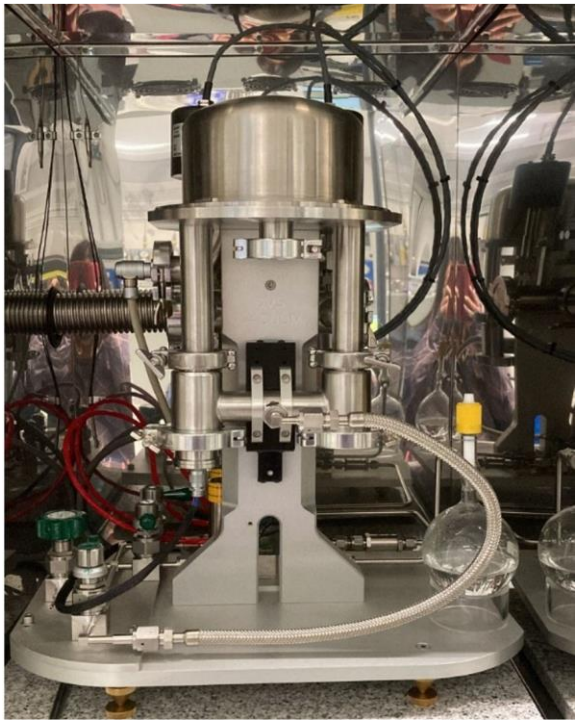

*Figure 3.8: Dynamic Vapor Sorption (DVS) instrument.*

# 4. Results and discussion

## *4.1.PIM-1 and cPIM -1 characterization*

### 4.1.1. *Thermo-gravimetric analysis coupled with infrared spectroscopy (TGA – FT-IR)*

Thermo-gravimetric analysis coupled with infrared spectroscopy was carried out both for powders of PIM-1 and cPIM-1.

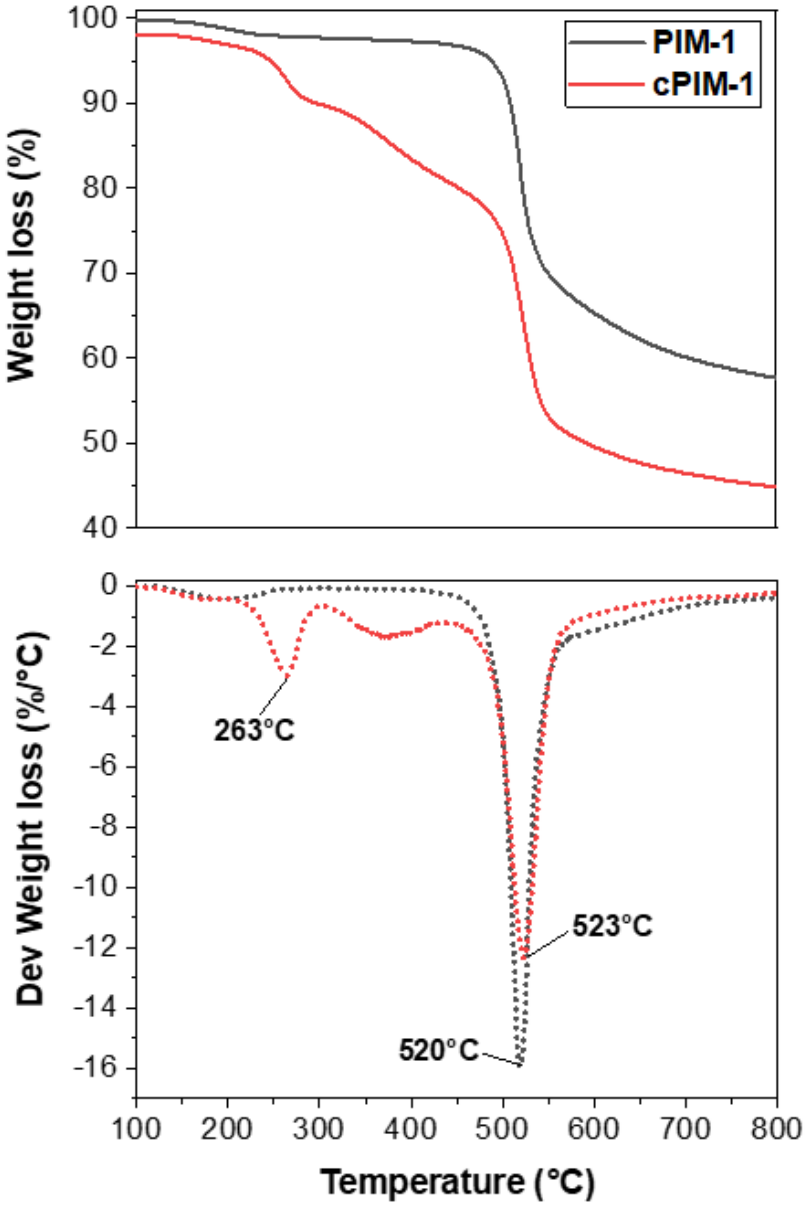


*Figure 4.1: TGA and DTGA of PIM-1 and cPIM-1.*

It is possible to observe from the first derivative of the TGA of PIM-1 a main weight loss at 520 °C, which can be accounted to the degradation of the organic matrix of PIM-1. A small weight loss at 190 °C is also present and from the IR plot at that temperature it was observed that this loss is related to NMP, in fact a signal is present around 1700 $cm^{-1}$ typical of the C=O double bond.

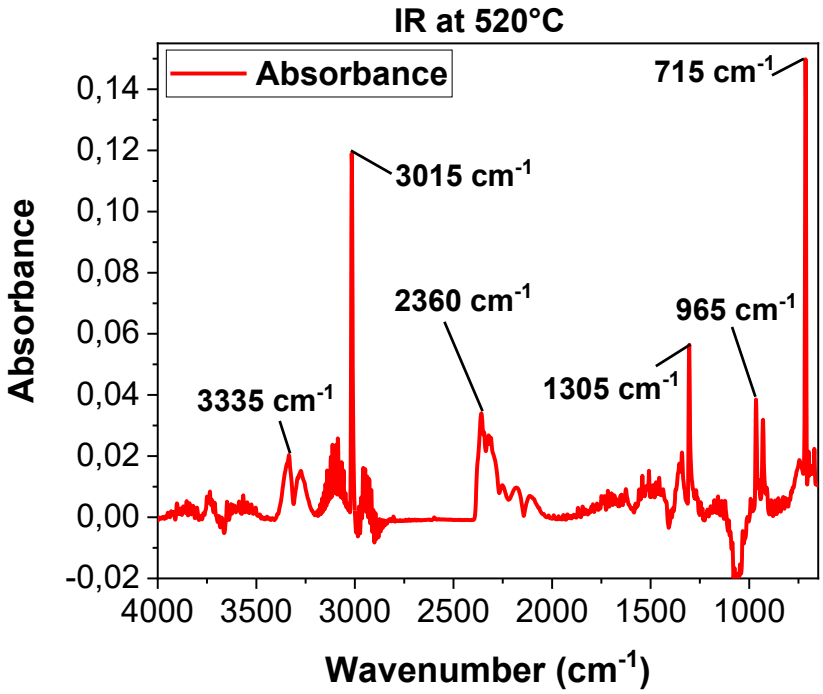


*Figure 4.2: FT-IR of PIM-1 at 520 °C.*

The signals present in the FT-IR plot of PIM-1 are the following [21]:

- at ~ 3000 $cm^{-1}$, related to the stretching of C-H with $sp^2$ and $sp^3$ hybridization;
- at 2360 $cm^{-1}$, related to the CN groups;
- at 1305 $cm^{-1}$, related to the stretching of the C-O bond.

The first derivative of TGA of cPIM-1 shows two weight losses at 263 °C and 523 °C.

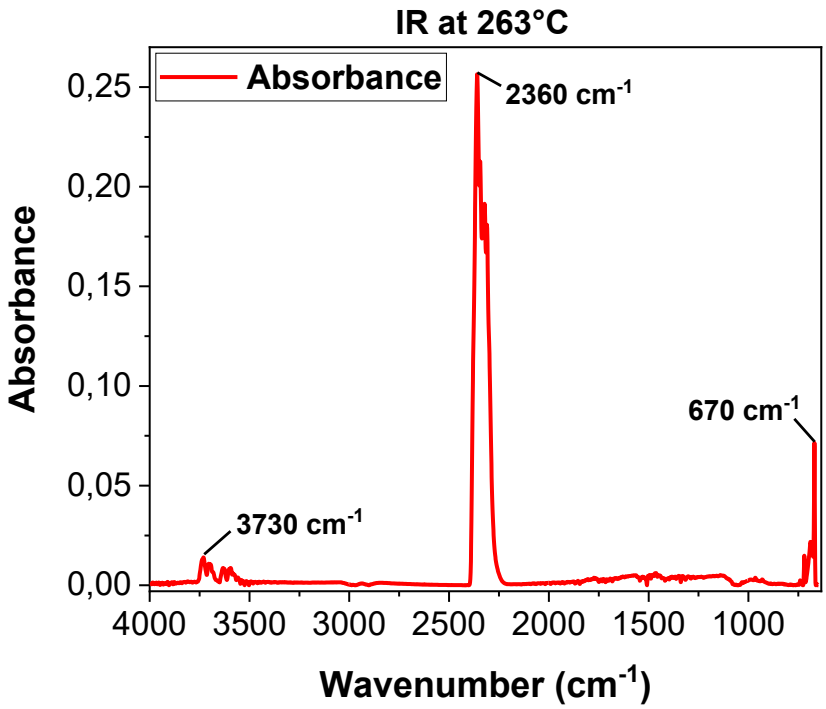


*Figure 4.3: FT-IR of cPIM-1 at 263 °C.*

The FT-IR of cPIM-1 at 263 °C shows a characteristic band present at 2360 $cm^{-1}$ that represents the $CO_2$ presence [19], this presence is confirmed from the absorbance at 3730 $cm^{-1}$ and 670 $cm^{-1}$. This signal confirms the obtained hydrolysis of PIM-1 bacause it is due to the decarbosilation of carboxylic acid formed.

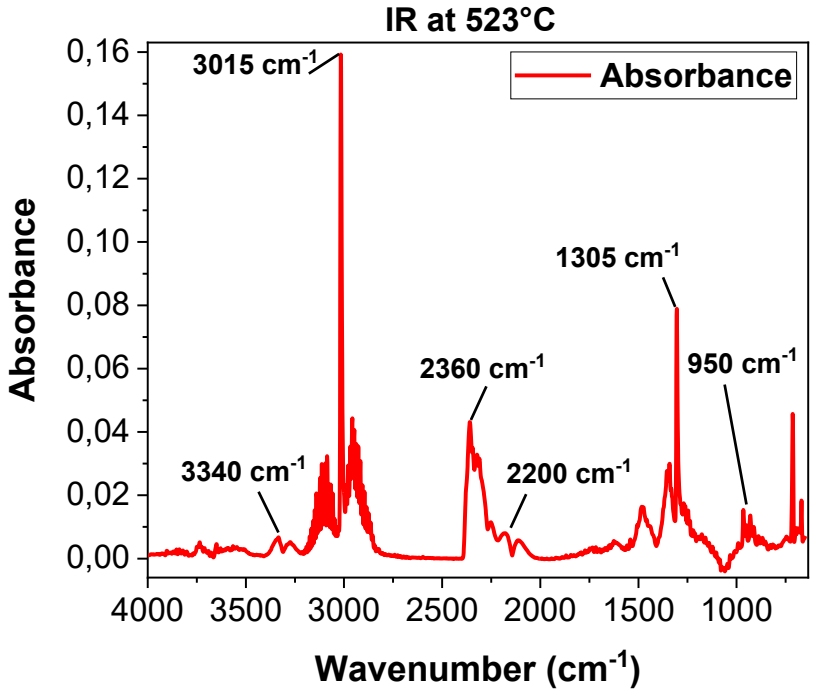


*Figure 4.4: FT-IR of cPIM-1 at 523 °C.*

It is possible to observe in the FT-IR of cPIM-1 at 523 °C typical signals at:

- 3015 $cm^{-1}$ and 1480 $cm^{-1}$, related to methane ($CH_4$);
- 2200 $cm^{-1}$, related to carbon monoxide (CO);
- 2360 $cm^{-1}$, related to carbon dioxide ($CO_2$);
- ~ 3400 $cm^{-1}$ (two humps) together with ~1000 $cm^{-1}$ (doublet), related to ammonia, ($NH_3$).

This second step is due to the degradation of the main PIM-1 chain, in a similar way that present for PIM-1.

### 4.1.2. *Infrared spectroscopy (FT-IR)*

The FT-IR was carried out with pads made with KBr and PIM-1 and cPIM-1.

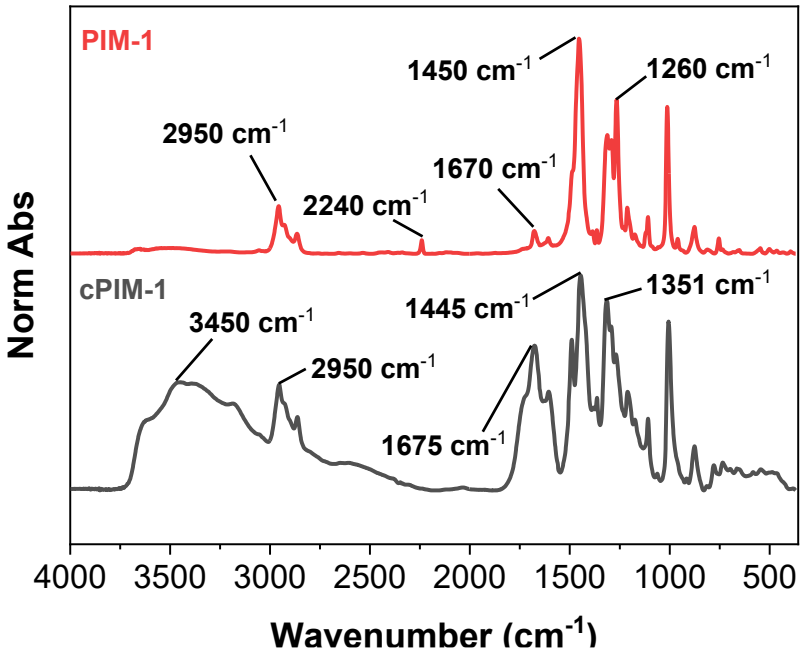


*Figure 4.5: FT-IR of PIM-1 and cPIM-1.*

It is possible to observe in Figure 4.5 the following signals [19]:

- at 1260 $cm^{-1}$ and 1315 $cm^{-1}$, due to stretching of the C-O bond;
- at 1450 $cm^{-1}$, due to stretching of the C=C bond;
- at 1675 $cm^{-1}$ the peak present in cPIM-1 is higher than that at 1670 $cm^{-1}$ present in PIM-1 due to the presence of the COOH group in cPIM-1. In particular, the signal at 1675 $cm^{-1}$ coupled with that at 3450 $cm^{-1}$, in cPIM-1, are related to the C=O (narrow band) and OH (broad band) bonds, respectively;
- at 2240 $cm^{-1}$ in PIM-1, due to the CN group, which instead disappears in cPIM-1 where it is not present;
- at 2950 $cm^{-1}$, due to stretching of the C-H bond with $sp^2$ and $sp^3$ hybridization.

### 4.1.3. *Differential scanning calorimetry (DSC)*

The samples were subjected to several heating/cooling cycles. To determine eventual transitions such as glass transition temperatures The first cycle from room temperature to 150 °C was made to clear the thermal history of the sample. As shown in Figures 4.6 and 4.7 (left diagrams) relative respectively to PIM-1 and cPIM-1, this cycle has a different slope than the others. Specifically, going to analyze the last heating cycle of both PIM-1 and cPIM-1 (right diagrams) and the first derivative with respect to temperature, which is more sensitive to any inflection points, no differences can be seen, an indication that there are no phase transitions in the range considered.

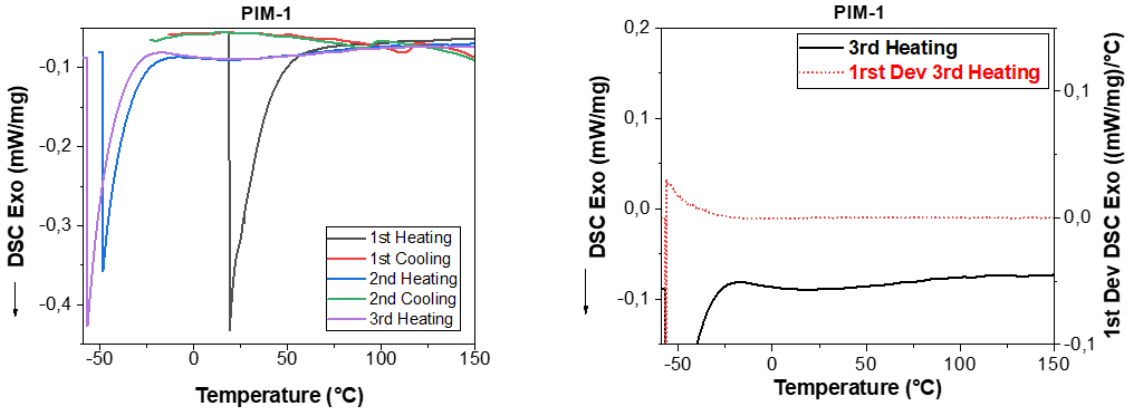


*Figure 4.6: DSC analysis of PIM-1; on the left: whole analysis with three heating cycles and two cooling cycles; on the right: last heating cycle.*

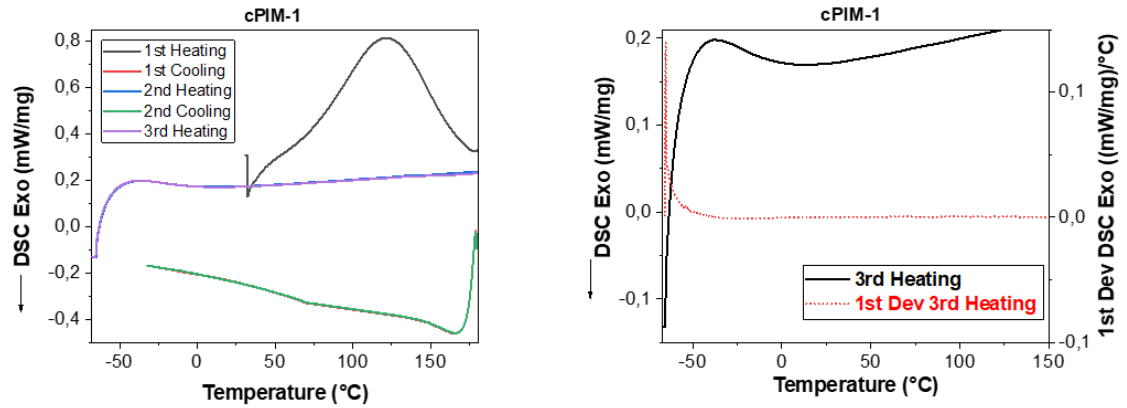


*Figure 4.7: DSC analysis of cPIM-1; on the left: whole analysis with three heating cycles and two cooling cycles; on the right: last heating cycle.*

## *4.2. Carbons characterization*

### 4.2.1. *Thermo-gravimetric analysis (TGA)*

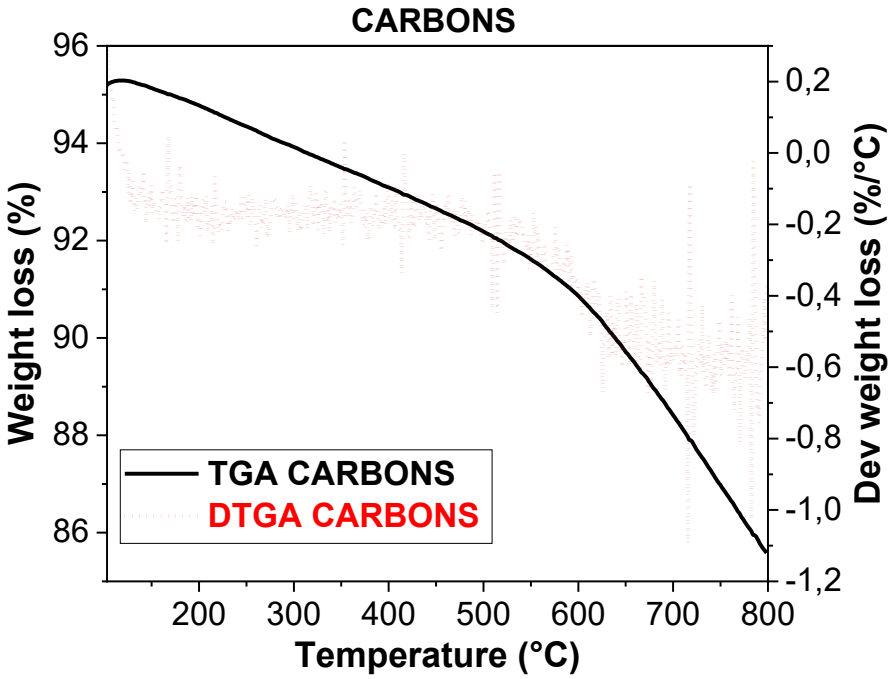


*Figure 4.8: TGA of CTOP600_MW biochar.*

From the thermogravimetric analysis of carbons, shown in Figure 4.8, it is possible to observe an initial weight loss of ~ 5 % at 100 °C related to solvents and/or humidity, and an additional weight loss of ~5%, between 600 °C and 800 °C, related to the impurities and imperfections of the crystalline lattice of carbons.

### 4.2.2. *Infrared spectroscopy (FT-IR)*

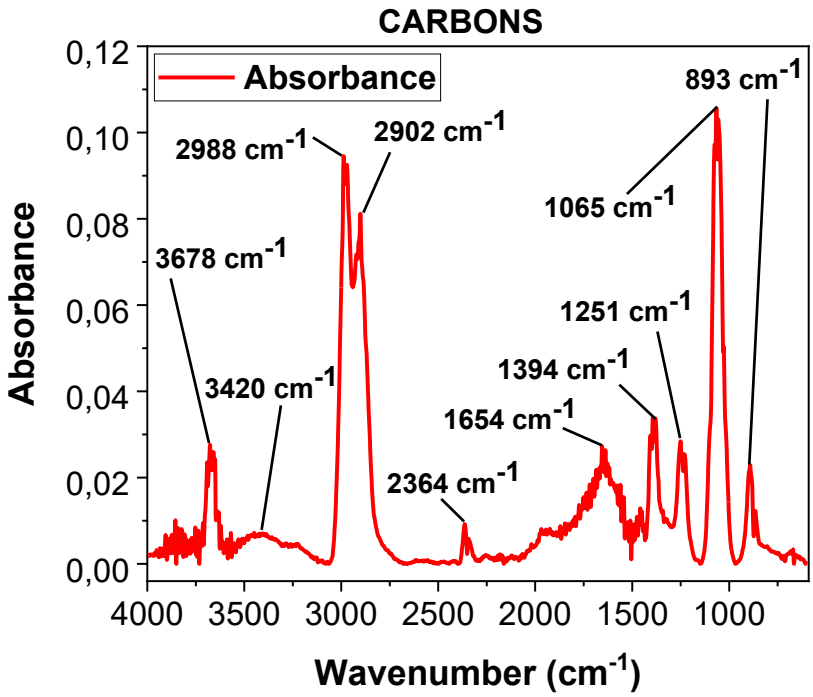


*Figure 4.9: FT-IR of CTOP600_MW biochar.*

The main characteristic signals present in the FT-IR of carbons and shown in Figure 4.9 are:

- at 3678 $cm^{-1}$, related to free O-H, and at 3420 $cm^{-1}$ , related to $NH_2$. These two signals derive from chitosan structure, the reagent used for the synthesis of carbons.
- at ~ 3000 $cm^{-1}$, due to stretching of the C-H bond with $sp^3$ hybridization;
- at 1065 $cm^{-1}$, due to stretching of the C-O bond;
- at 1654 $cm^{-1}$, related to C=O bond;
- at 2364 $cm^{-1}$, related to the CN groups;
- at 1394 $cm^{-1}$ and 1251 $cm^{-1}$, related to the bending of C-H ($CH_2$, $CH_3$);
- at 893 $cm^{-1}$, due to the bending of C-H.

### 4.2.3. *Differential scanning calorimetry (DSC)*

The DSC analysis of carbons was conducted in the same way as described in section 4.1.3 but by performing a pretreatment before. In fact, carbons were firstly preheated at 120 °C for 1 h and 30 min, by putting them in a vacuum system (Buchi).

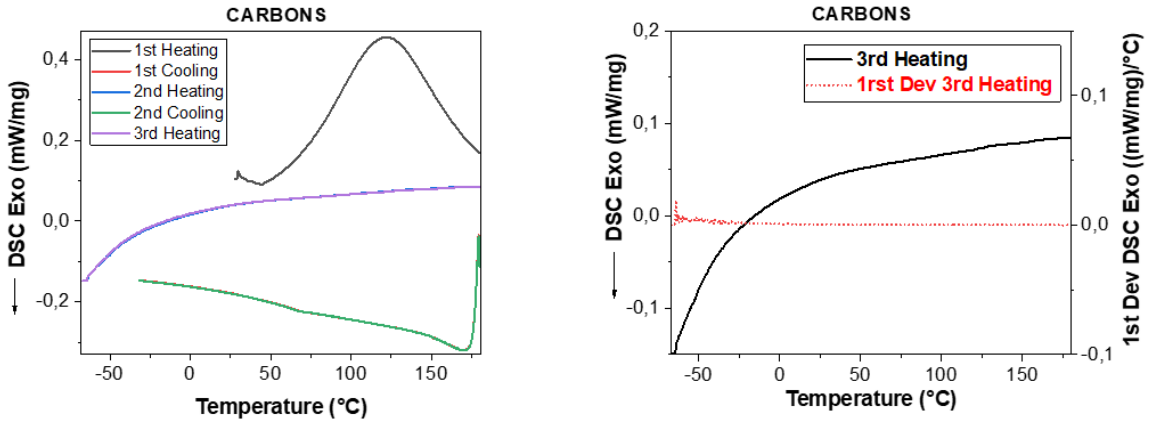


*Figure 4.10: DSC of CTOP600_MW biochar.*

It is possible to observe that the first derivative with respect to temperature of the third heating cycle, shown in Figure 4.10 (right diagram), does not present peaks and the slope is constant with the increase of temperature meaning that there are no phase transitions in the range considered.

## *4.3.cPIM-1 based membrane*

The cPIM-1 was filmed in order to optimise the membrane production using several solvents and in different conditions, the results were summarised in the section 11.1, based on the results obtained from of all the tests performed, the best solution is represented by the membrane of cPIM-1 realized with NMP, as solvent, and on LDPE, as support. It turns out to be flexible and without micro fractures, as shown in Figure 4.11.


*Figure 4.11: cPIM-1 membrane realized in NMP and LDPE.*

The average density and the average thickness of the cPIM-1 membrane were calculated. The results are the following:

| **Membrane** | **Average thickness (cm)** | **Average density ($g/cm^3$)** |
|---|---|---|
| **cPIM-1** | $0.006 \pm 0.001$ | $1.197 \pm 0.029$ |

*Table 4.1: Average thickness and average density of cPIM-1 membrane.*

## *4.4.cPIM-1 with carbons-based membrane*

The cPIM-1 membranes with different percentages of carbons, 5%, 2% and 1%, were realized by applying the optimal production procedure that involves the use of NMP, as solvent, and LDPE, as support. The membranes result plastics and without evident micro fractures, as shown in Figure 4.12.

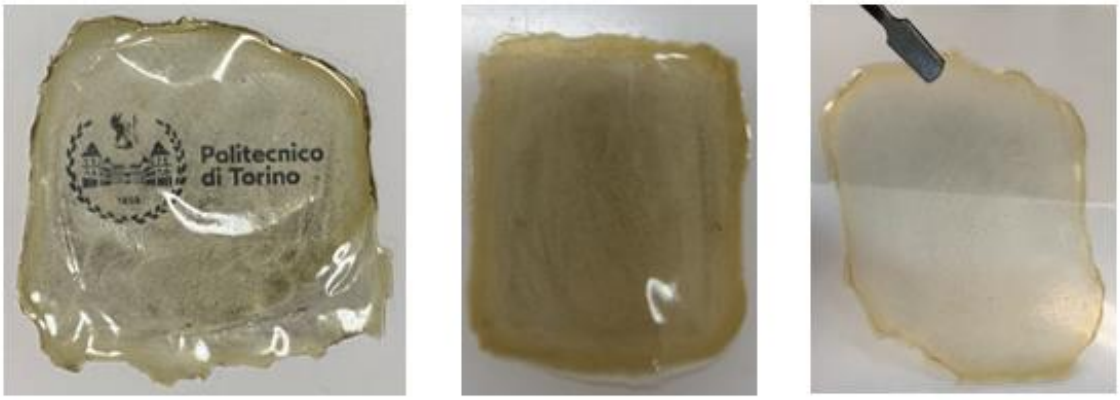


*Figure 4.12: Membranes of cPIM-1 with 5 % carbons (on the left), 2 % carbons (at the center), 1 % carbons (on the right) realized on LDPE.*

The average density and the average thickness of the cPIM-1 with carbons-based membranes were calculated. The results are the following:

| **Membrane** | **Average thickness (cm)** | **Average density ($g/cm^3$)** |
|---|---|---|
| **cPIM-1 with 5% carbons w/w** | $0.004 \pm 0.001$ | $1.214 \pm 0.119$ |
| **cPIM-1 with 2% carbons w/w** | $0.006 \pm 0.001$ | $1.065 \pm 0.104$ |
| **cPIM-1 with 1% carbons w/w** | $0.007 \pm 0.001$ | $1.120 \pm 0.044$ |

*Table 4.2: Average thickness and average density of cPIM-1 membrane with 5%, 2%, 1% carbons w/w.*

## *4.5.Membranes characterization*

### 4.5.1. *Thermo-gravimetric analysis coupled with infrared spectroscopy (TGA – FT-IR)*

Thermo-gravimetric analysis coupled with infrared spectroscopy was carried out for all the membranes and the comparison of the curves obtained can be observed in Figure 4.13.

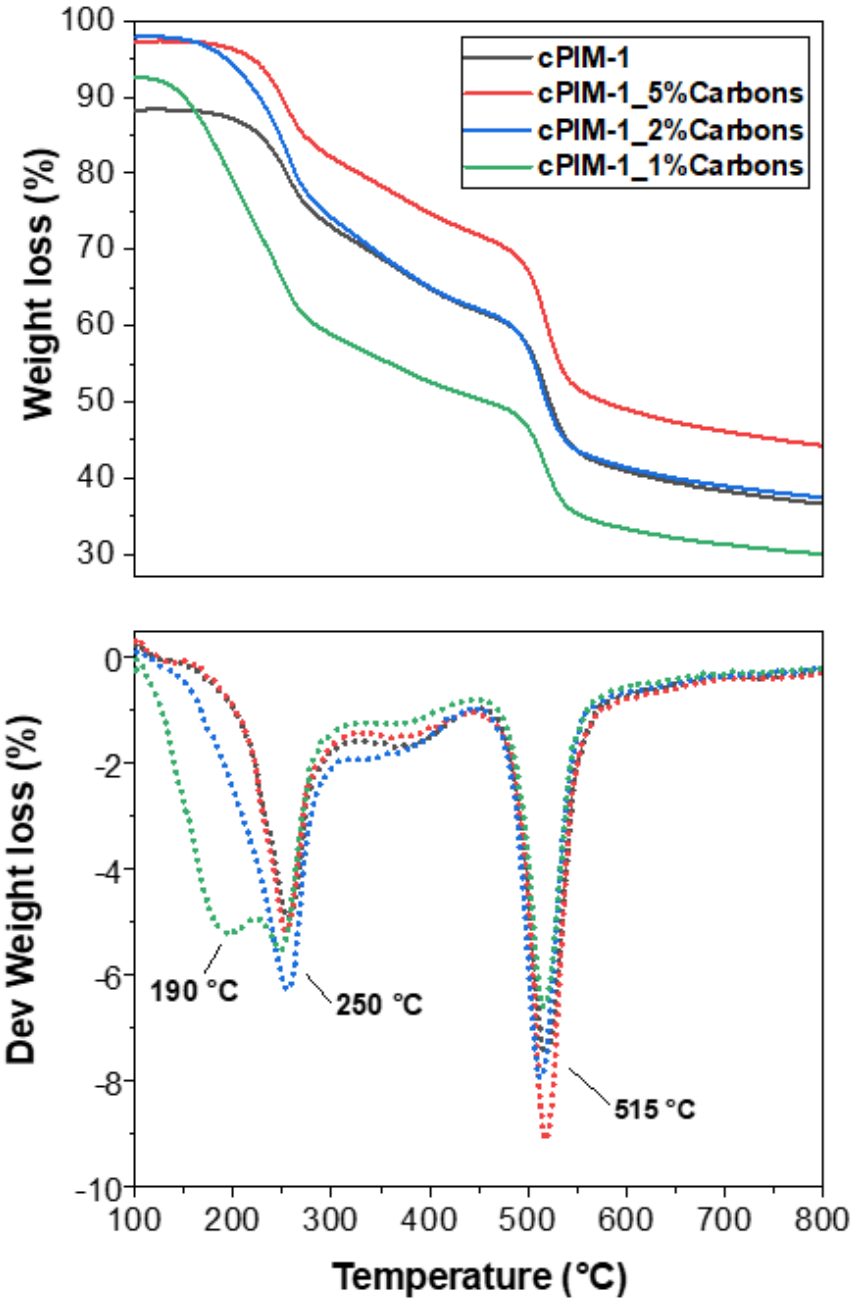


*Figure 4.13: TGA and DTGA of membranes.*

The main steps of weight loss are:

- 190 °C, related to the presence of solvents (only evident in cPIM-1_5%Carbons),
- 250 °C, related to the carboxyl functional groups,
- 515 °C, related to the degradation of the main chain of PIM-1.

The first derivative of the TGA shows two weight losses very similar to cPIM-1 alone, only in the case of cPIM-1 with 5% of carbons there is a weight loss around 190°C.

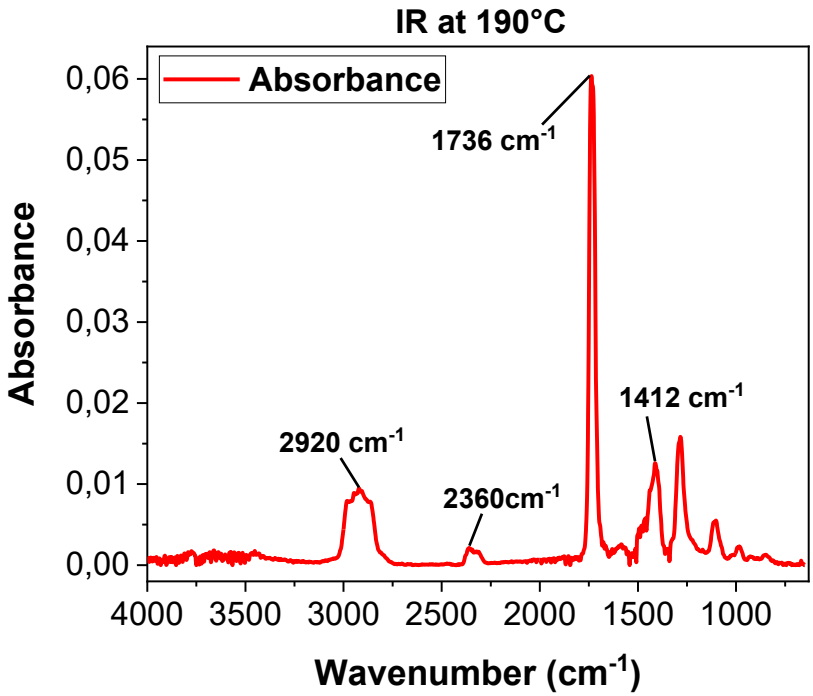


*Figure 4.14: FT-IR of cPIM-1 membrane with 1% carbons w/w at 190 °C.*

The FT-IR plot of cPIM-1 membrane with 1% carbons at 190 °C presents the typical signals of the solvent 1-metil-2-pirrolidone, NMP, as demonstrated in the IR spectrum extracted from NIST, National Institute of Standards and Technology, Chemistry WebBook and shown in Figure 4.15.

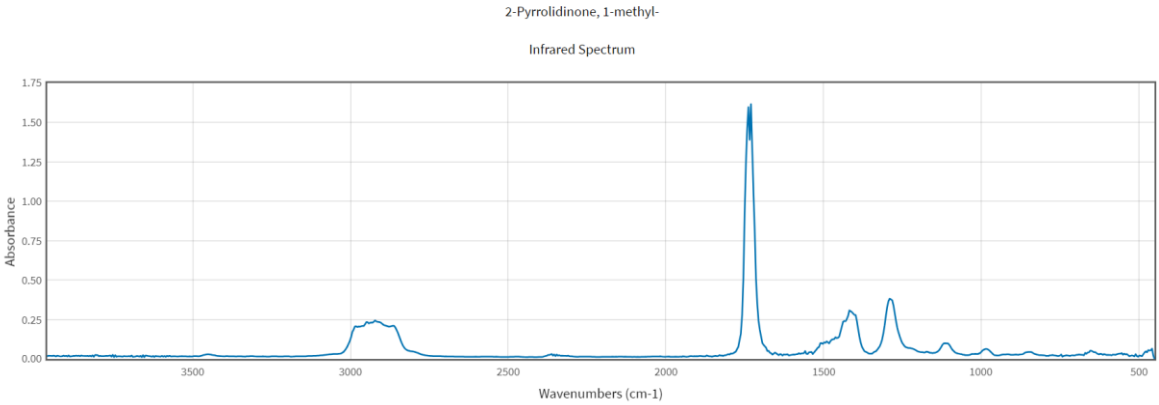


*Figure 4.15: IR spectrum of NMP extracted from NIST Chemistry WebBook.*

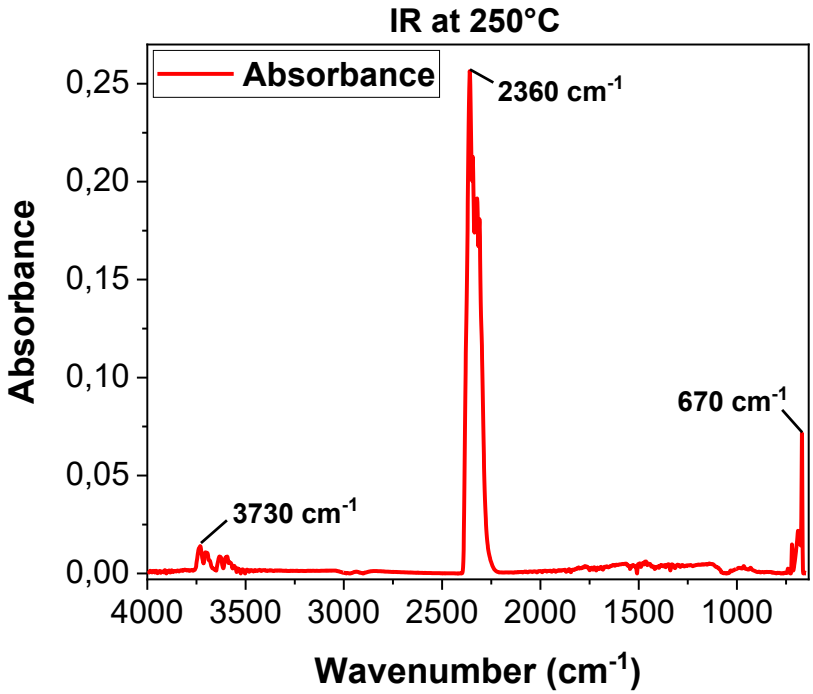


*Figure 4.16: FT-IR of cPIM-1 membrane and cPIM-1 membranes with 5%, 2%, 1% of carbons w/w at 250 °C.*

The FT-IR plot of membranes at 250 °C presents a characteristic band at 2360 $cm^{-1}$ that represents the relative contribution to the $CO_2$ difference between background and sample [19]. The presence of $CO_2$ is also represented by the two humps at 3730 $cm^{-1}$ also coupled to the 670 $cm^{-1}$ signal.

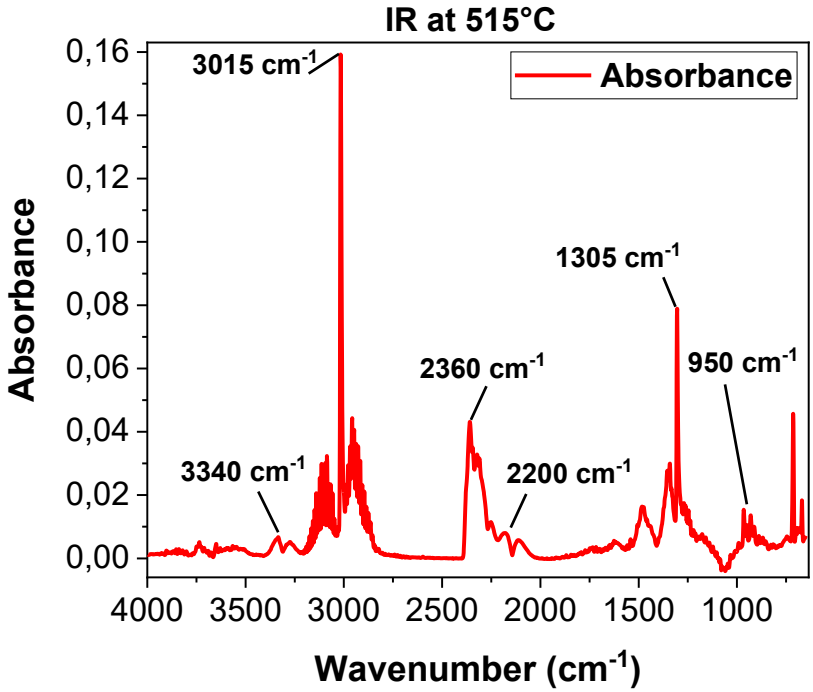


*Figure 4.17: FT-IR of cPIM-1 membrane and cPIM-1 membranes with 5%, 2%, 1% of carbons w/w at 515 °C.*

The typical signals shown in the FT-IR plot of all the membranes at 515 °C are:

- at 3015 $cm^{-1}$ and 1480 $cm^{-1}$, related to methane, $CH_4$,
- at 2200 $cm^{-1}$, related to carbon monoxide, CO,
- at 2360 $cm^{-1}$, related to carbon dioxide, $CO_2$,
- at ~ 3400 $cm^{-1}$ (two humps) together with ~1000 $cm^{-1}$ (doublet), related to ammonia, $NH_3$.

### 4.5.2. *Infrared spectroscopy (FT-IR)*

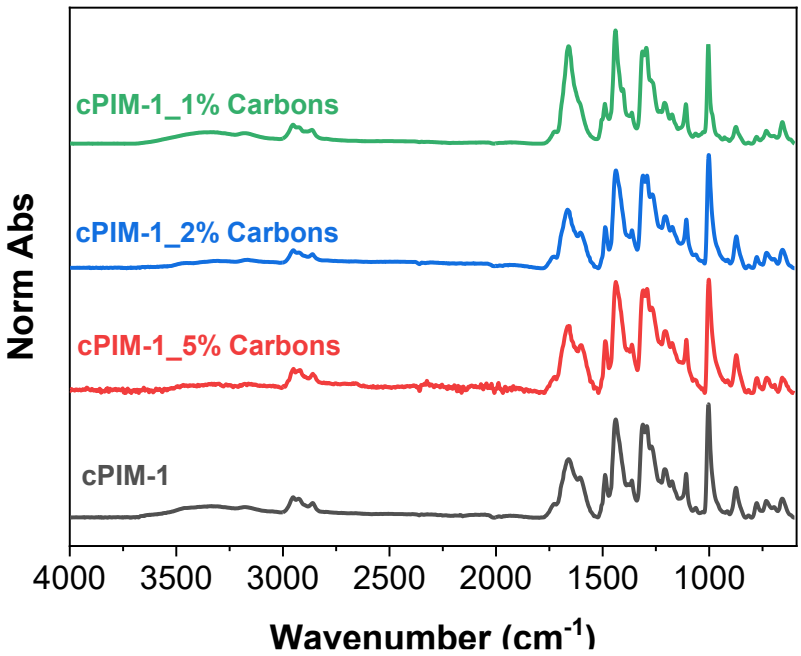


*Figure 4.18: FT-IR of membranes.*

Comparing the results of the FT-IR analysis performed for all membranes, it is possible to observe that there are no differences in signals of the cPIM-1 membrane with respect to the cPIM-1 membranes with different percentages of carbons, as shown in Figure 4.18.

### 4.5.3. *Differential scanning calorimetry (DSC)*

The DSC analysis was conducted for the cPIM-1 membrane and the cPIM-1 membranes with 5%, 2%, 1% of carbons.

Based on the results obtained, shown in Figures below, it is possible to state that there are no phase transitions, as visible from the first derivative with respect to temperature of the third heating cycle.

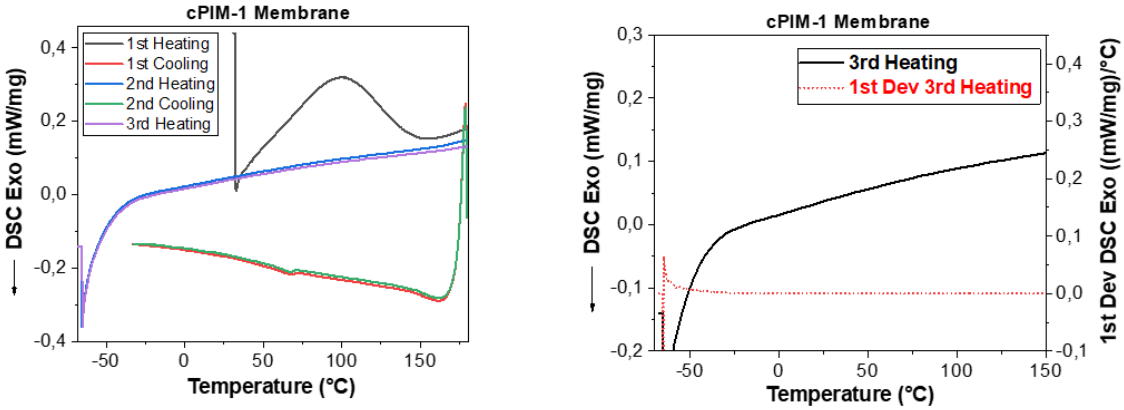


*Figure 4.19: DSC analysis of cPIM-1 membrane; on the left: whole analysis with three heating cycles and two cooling cycles; on the right: last heating cycle.*

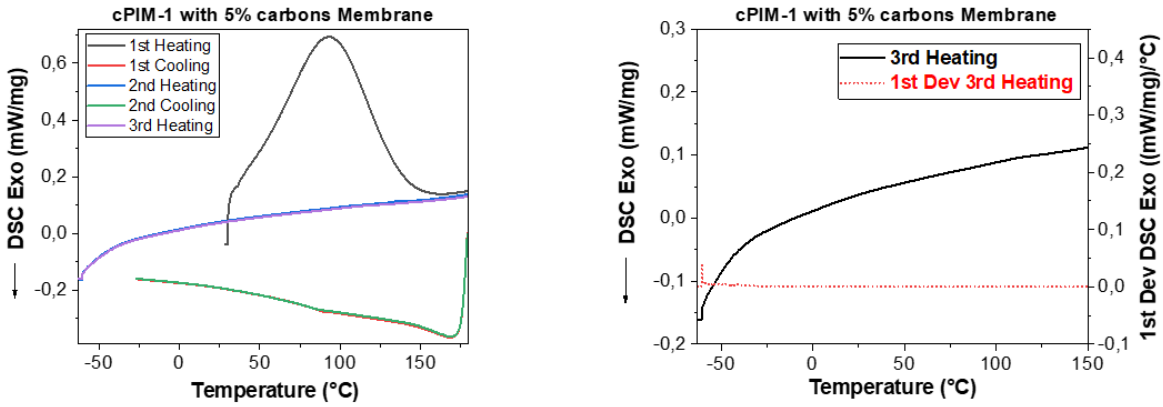


*Figure 4.20: DSC analysis of cPIM-1 membrane with 5% carbons w/w; on the left: whole analysis with three heating cycles and two cooling cycles; on the right: last heating cycle.*

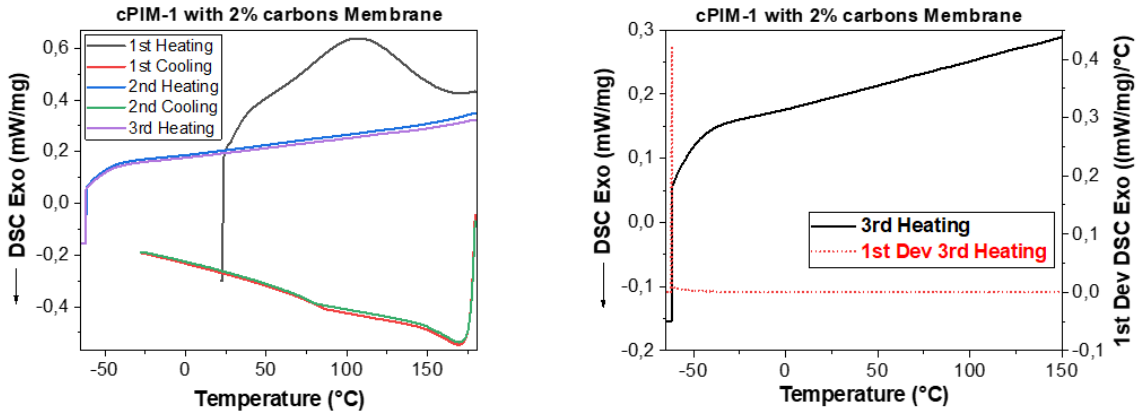


*Figure 4.21: DSC analysis of cPIM-1 membrane with 2% carbons w/w; on the left: whole analysis with three heating cycles and two cooling cycles; on the right: last heating cycle.*

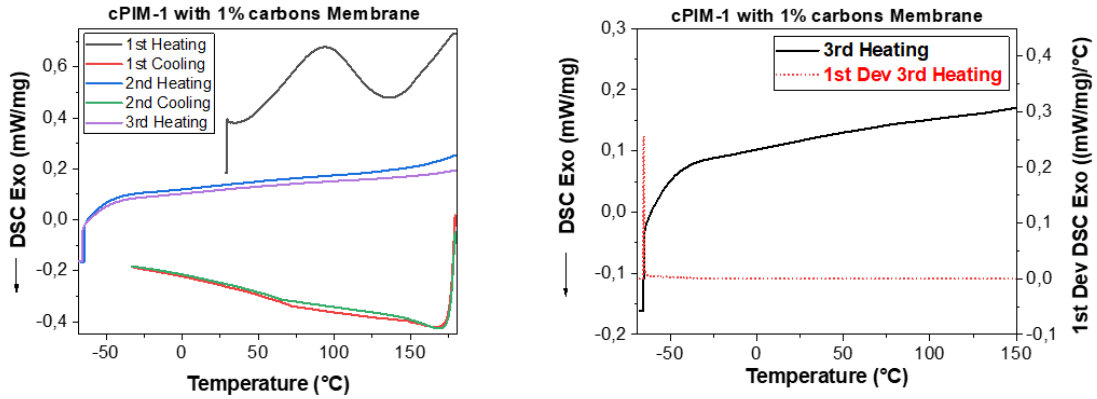


*Figure 4.22: DSC analysis of cPIM-1 membrane with 1% carbons w/w; on the left: whole analysis with three heating cycles and two cooling cycles; on the right: last heating cycle.*

### 4.5.4. *Field Emission Scanning Electron Microscopy (FESEM) of membranes*

Field emission scanning electron microscopy (FE-SEM) was used to analyse the surface morphology of fabricated membranes reported in the Figures below.

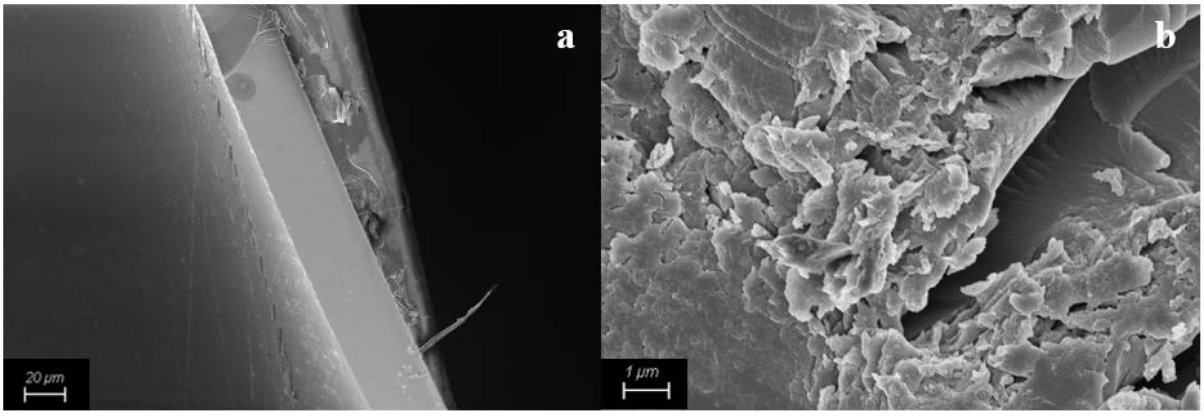


*Figure 4.23: FESEM of cPIM-1 membrane.*

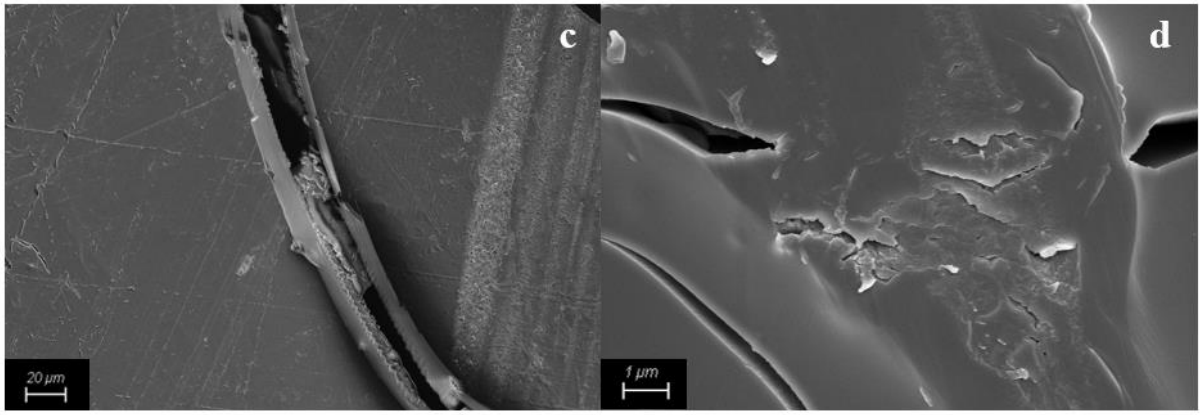


*Figure 4.24: FESEM of cPIM-1 membrane with 5% carbons w/w.*

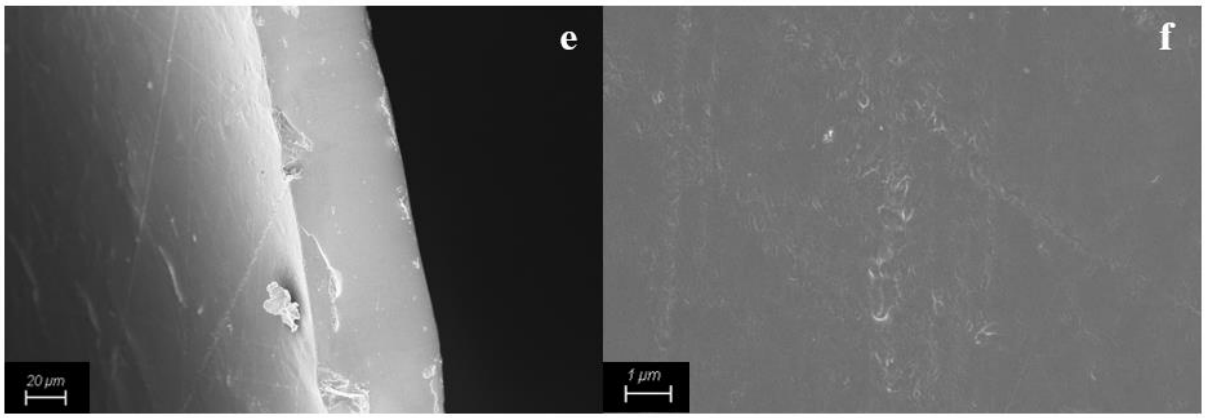


*Figure 4.25: FESEM of cPIM-1 membrane with 2% carbons w/w.*

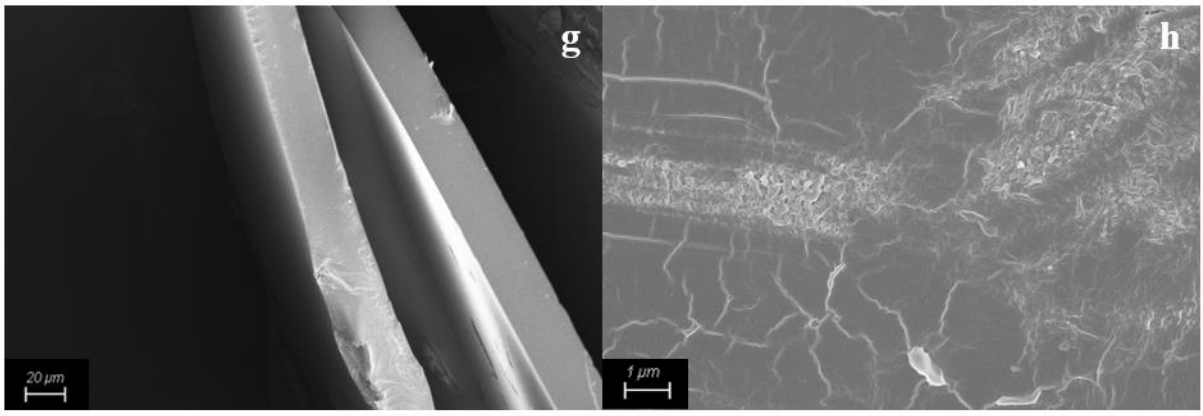


*Figure 4.26: FESEM of cPIM-1 membrane with 1% carbons w/w.*

The main difference between the cPIM-1 membrane and the cPIM-1 membranes with 5%, 2%, 1% of carbons is that the first one presents a spongy surface with interconnected pores, as shown in Figure 4.23 b, whereas the second ones present a smoother surface, as shown in Figures 4.24 d, 4.25 f and 4.26 h.

FESEM was also used to calculate the average thickness of the membranes.

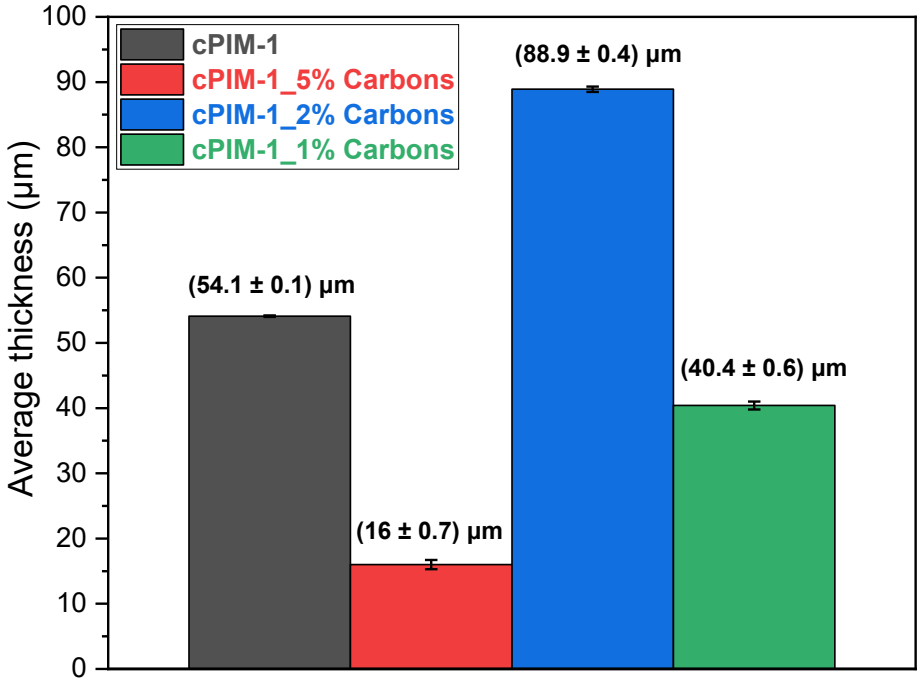


*Figure 4.27: Average thickness of membranes obtained from FESEM.*

Based on the results obtained, it is possible to state that the membranes present different thicknesses, as shown in Figure 4.27.

# 5. Dynamic Vapor Sorption (DVS) instrument

Permeabilities were studied using gases adsorption through microbalance, assessing the weight gain from the membranes and knowing their geometry it was possible to evaluate permeability, diffusion coefficients and solubility of the different gases.

## *5.1. $CO_2$ permeability parameters of MMM*

In Figure 5.1, the performance of various membranes for $CO_2$ transport is presented. The permeability of $CO_2$ appears fairly consistent across different membranes at varying concentrations. However, an increase in carbon content within these membranes correlates with an increased solubility of $CO_2$, peaking at a carbon content of 5.0 wt%. It's important to note that the method used for measuring permeability may not be as effective for extremely high permeability scenarios, such as those observed with PIMs membranes, while solubility measurements remain reliable. Therefore, the observed increase in $CO_2$ solubility, especially at higher carbon contents, is particularly noteworthy.

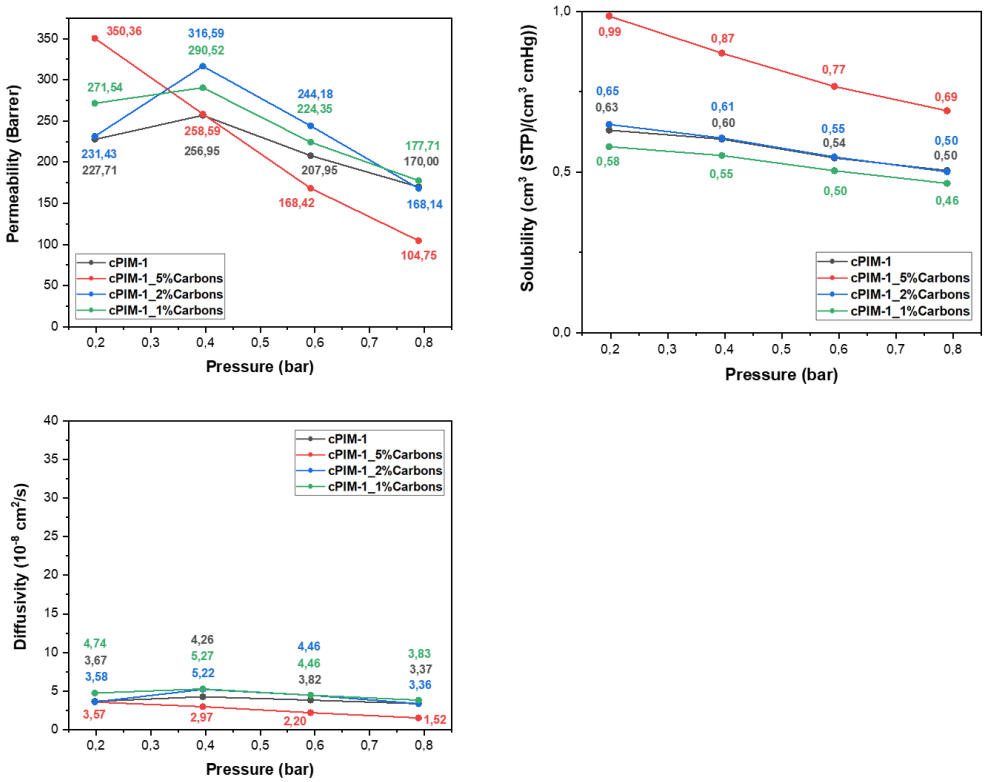


*Figure 5.1: Comparison of membranes of cPIM-1, cPIM-1 with 5% carbons w/w, cPIM-1 with 2% carbons w/w and cPIM-1 with 1% carbons w/w at different $CO_2$ partial gas pressures.*

| Membrane | $CO_2$ Pressure (bar) | Permeability (Barrer) | Diffusivity ($10^{-8}$ $cm^2/s$) | Solubility ($cm^3$ (STP)/$cm^3$ cmHg) |
|---|---|---|---|---|
| **cPIM-1** | 0.2 | 227.71 ± 68.81 | 3.67 ± 1.36 | 0.630 ± 0.042 |
| | 0.4 | 256.95 ± 10.06 | 4.26 ± 0.09 | 0.603 ± 0.011 |
| | 0.6 | 207.95 ± 12.63 | 3.82 ± 0.16 | 0.544 ± 0.008 |
| | 0.8 | 170 ± 21.53 | 3.37 ± 0.38 | 0.505 ± 0.008 |
| **cPIM-1 with 5% Carbons** | 0.2 | 350.36 ± 202.75 | 3.57 ± 2.11 | 0.985 ± 0.012 |
| | 0.4 | 258.59 ± 4.11 | 2.97 ± 0.05 | 0.869 ± 0.004 |
| | 0.6 | 168.42 ± 3.13 | 2.19 ± 0.03 | 0.766 ± 0.004 |
| | 0.8 | 104.75 ± 4.23 | 1.52 ± 0.05 | 0.691 ± 0.005 |
| **cPIM-1 with 2% Carbons** | 0.2 | 231.43 ± 49.31 | 3.58 ± 0.80 | 0.648 ± 0.011 |
| | 0.4 | 316.59 ± 17.58 | 5.22 ± 0.21 | 0.606 ± 0.008 |
| | 0.6 | 244.18 ± 28.60 | 4.46 ± 0.45 | 0.547 ± 0.008 |
| | 0.8 | 168.14 ± 9.99 | 3.36 ± 0.16 | 0.501 ± 0.006 |
| **cPIM-1 with 1% Carbons** | 0.2 | 271.54 ± 55.93 | 4.74 ± 1.22 | 0.579 ± 0.032 |
| | 0.4 | 290.52 ± 38.75 | 5.27 ± 0.74 | 0.552 ± 0.009 |
| | 0.6 | 224.35 ± 25.06 | 4.46 ± 0.58 | 0.504 ± 0.009 |
| | 0.8 | 177.71 ± 18.27 | 3.83 ± 0.41 | 0.465 ± 0.008 |

*Table 5.1: Permeability, diffusivity and solubility data of membranes of cPIM-1, cPIM-1 with 5% carbons w/w, cPIM-1 with 2% carbons w/w and cPIM-1 with 1% carbons w/w at different $CO_2$ partial gas pressures.*

## *5.2. $CH_4$ permeability parameters of MMM*

In Figure 5.2, the performance of various membranes in methane ($CH_4$) transport is reported. The permeability of methane is relatively consistent across different membranes at various concentrations, with an exception observed at very high concentrations of methane for the membrane containing 5 wt% of carbon. In this scenario, an increase in carbon content notably reduces the solubility of $CH_4$, thereby enhancing the separation characteristics of the membranes. However, it's also noted that the method employed does not perform optimally for extremely high permeability cases, such as those observed with PIMs membranes. Consequently, for accurate assessment of diffusivity and permeability, the use of more advanced and capable instruments is recommended.

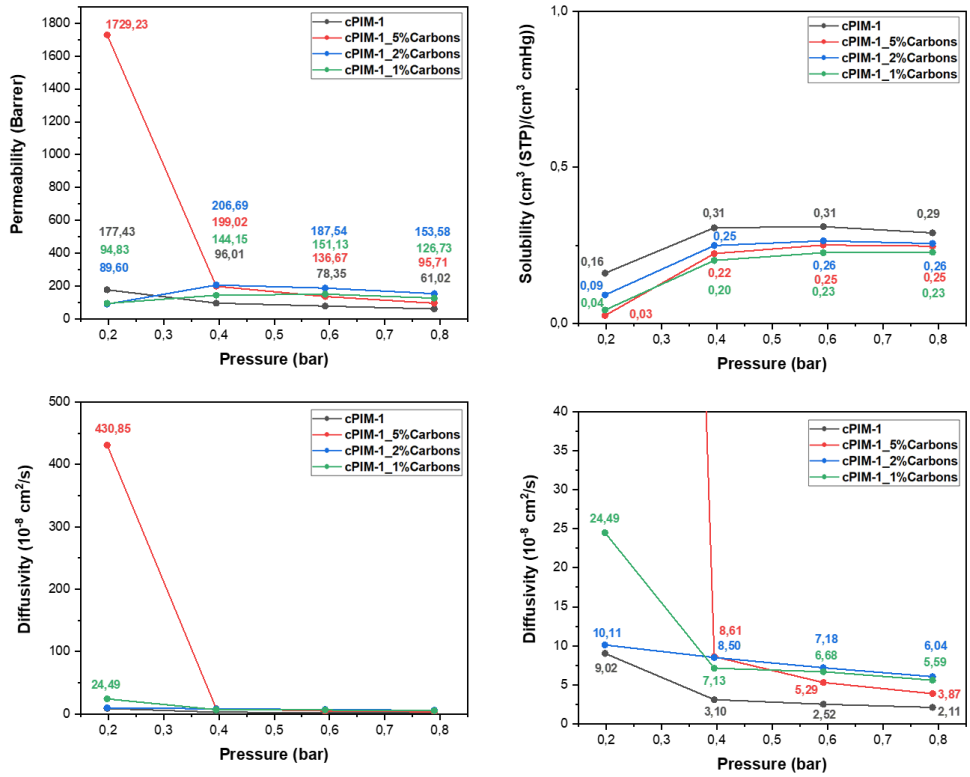


*Figure 5.2: Comparison of membranes of cPIM-1, cPIM-1 with 5% carbons w/w, cPIM-1 with 2% carbons w/w and cPIM-1 with 1% carbons w/w at different $CH_4$ partial gas pressures.*

| Membrane | $CH_4$ Pressure (bar) | Permeability (Barrer) | Diffusivity ($10^{-8}$ $cm^2/s$) | Solubility ($cm^3$ (STP)/$cm^3$ cmHg) |
|---|---|---|---|---|
| **cPIM-1** | 0.2 | 177.43 ± 263.42 | 9.02 ± 10.21 | 0.161 ± 0.042 |
| | 0.4 | 96.02 ± 20.97 | 3.10 ± 0.32 | 0.307 ± 0.034 |
| | 0.6 | 78.35 ± 12.42 | 2.52 ± 0.17 | 0.31 ± 0.030 |
| | 0.8 | 61.02 ± 5.14 | 2.11 ± 0.12 | 0.290 ± 0.025 |
| **cPIM-1 with 5% Carbons** | 0.2 | 1729.23 ± 2887.00 | 431 ± 682.49 | 0.025 ± 0.040 |
| | 0.4 | 199.02 ± 160.61 | 8.61 ± 6.19 | 0.224 ± 0.029 |
| | 0.6 | 136.68 ± 63.12 | 5.29 ± 1.91 | 0.251 ± 0.027 |
| | 0.8 | 95.71 ± 30.05 | 3.87 ± 1.14 | 0.248 ± 0.025 |
| **cPIM-1 with 2% Carbons** | 0.2 | 89.59 ± 11.23 | 10.11 ± 2.26 | 0.091 ± 0.022 |
| | 0.4 | 206.69 ± 122.00 | 8.49 ± 5.57 | 0.249 ± 0.014 |
| | 0.6 | 187.54 ± 42.75 | 7.18 ± 2.13 | 0.265 ± 0.017 |
| | 0.8 | 153.58 ± 21.97 | 6.04 ± 1.11 | 0.256 ± 0.017 |
| **cPIM-1 with 1% Carbons** | 0.2 | 94.83 ± 119.59 | 24.49 ± 26.85 | 0.043 ± 0.073 |
| | 0.4 | 144.15 ± 25.59 | 7.13 ± 0.39 | 0.202 ± 0.032 |
| | 0.6 | 151.13 ± 40.19 | 6.68 ± 1.85 | 0.227 ± 0.019 |
| | 0.8 | 126.73 ± 24.01 | 5.59 ± 1.20 | 0.228 ± 0.014 |

*Table 5.2: Permeability, diffusivity and solubility data of membranes of cPIM-1, cPIM-1 with 5% carbons w/w, cPIM-1 with 2% carbons w/w and cPIM-1 with 1% carbons w/w at different $CH_4$ partial gas pressures.*

## *5.3.$N_2$ permeability parameters of MMM*

In Figure 5.3, the performance of various membranes in nitrogen transport is detailed. The permeability of nitrogen appears relatively consistent across different membranes at varying concentrations, with a notable exception being the membrane containing 1 wt% of carbon at low pressure. Interestingly, an increase in carbon content leads to a decreased solubility of $N_2$ in membranes with 2 wt% and 1 wt% carbon, whereas it remains quite similar in the 5 wt% carbon membrane. This implies that the ratio of $CO_2$ to $N_2$ adsorption increases in the presence of carbon, thereby enhancing the membrane's efficacy for $CO_2$ separation.

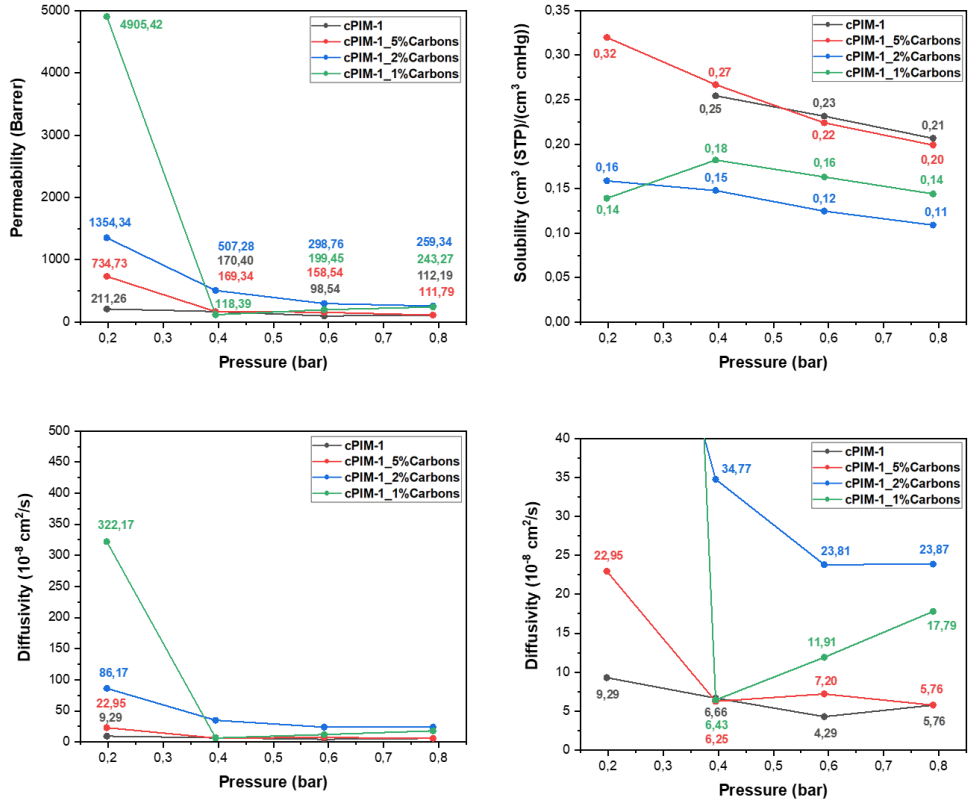


*Figure 5.3: Comparison of membranes of cPIM-1, cPIM-1 with 5% carbons w/w, cPIM-1 with 2% carbons w/w and cPIM-1 with 1% carbons w/w at different $N_2$ partial gas pressures.*

| Membrane | $N_2$ Pressure (bar) | Permeability (Barrer) | Diffusivity ($10^{-8}$ $cm^2/s$) | Solubility ($cm^3$ (STP)/$cm^3$ cmHg) |
|---|---|---|---|---|
| **cPIM-1** | 0.2 | 211.26 ± 51.83 | 9.29 ± 2.17 | 0.227 ± 0.018 |
| | 0.4 | 170.40 ± 33.07 | 6.66 ± 0.76 | 0.254 ± 0.026 |
| | 0.6 | 98.54 ± 4.12 | 4.29 ± 0.40 | 0.231 ± 0.025 |
| | 0.8 | 112.19 ± 77.04 | 5.76 ± 4.66 | 0.207 ± 0.023 |
| **cPIM-1 with 5% Carbons** | 0.2 | 734.74 ± 574.58 | 22.95 ± 13.20 | 0.319 ± 0.163 |
| | 0.4 | 169.34 ± 56.54 | 6.25 ± 0.65 | 0.267 ± 0.066 |
| | 0.6 | 158.54 ± 13.74 | 7.20 ± 1.06 | 0.224 ± 0.041 |
| | 0.8 | 111.79 ± 18.96 | 5.76 ± 1.61 | 0.199 ± 0.032 |
| **cPIM-1 with 2% Carbons** | 0.2 | 1354.34 ± 98.37 | 86.17 ± 12.80 | 0.159 ± 0.019 |
| | 0.4 | 507.28 ± 153.80 | 34.77 ± 12.35 | 0.148 ± 0.011 |
| | 0.6 | 298.76 ± 82.23 | 23.81 ± 5.76 | 0.125 ± 0.007 |
| | 0.8 | 259.34 ± 101.38 | 23.87 ± 9.31 | 0.109 ± 0.008 |
| **cPIM-1 with 1% Carbons** | 0.2 | 4905.42 ± 7494.64 | 322.17 ± 481.04 | 0.139 ± 0.014 |
| | 0.4 | 118.39 ± 37.64 | 6.43 ± 1.60 | 0.182 ± 0.012 |
| | 0.6 | 199.45 ± 194.27 | 11.91 ± 11.26 | 0.163 ± 0.010 |
| | 0.8 | 243.27 ± 215.32 | 17.79 ± 17.07 | 0.144 ± 0.011 |

*Table 5.3: Permeability, diffusivity and solubility data of membranes of cPIM-1, cPIM-1 with 5% carbons w/w, cPIM-1 with 2% carbons w/w and cPIM-1 with 1% carbons w/w at different $N_2$ partial gas pressures.*

## *5.1.$H_2$ permeability parameters of MMM*

In Figure 5.4, the performance of various membranes in hydrogen transport is presented. The enhanced solubility of hydrogen is likely due to its relatively small dynamic radius compared to other gases, facilitating faster transport. This is particularly evident in the presence of carbon, which contains small mesopores that allow hydrogen to pass through more readily while significantly slowing the entry of other gases. Notably, for all the membranes evaluated, hydrogen solubility is substantially higher than that of other gases, suggesting these membranes could be effectively utilized for the rapid separation of hydrogen from gas mixtures.

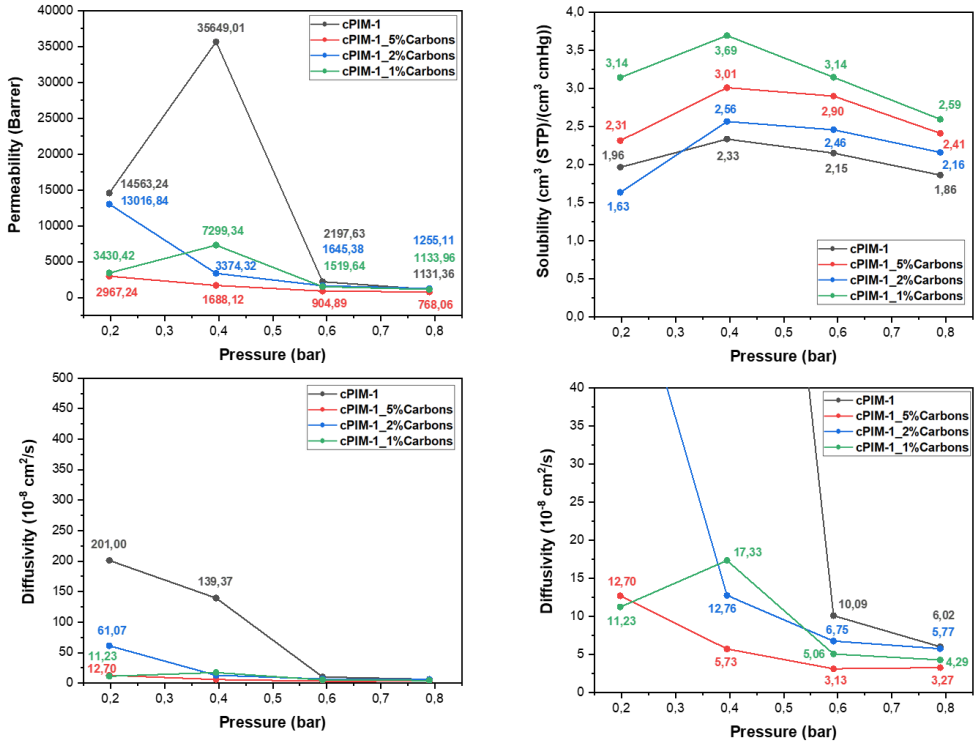


*Figure 5.4: Comparison of membranes of cPIM-1, cPIM-1 with 5% carbons w/w, cPIM-1 with 2% carbons w/w and cPIM-1 with 1% carbons w/w at different $H_2$ partial gas pressures.*

| Membrane | $H_2$ Pressure (bar) | Permeability (Barrer) | Diffusivity ($10^{-8}$ $cm^2/s$) | Solubility ($cm^3$ (STP)/$cm^3$ cmHg) |
|---|---|---|---|---|
| **cPIM-1** | 0.2 | 14563.24 ± 21723.85 | 200.99 ± 200.37 | 1.964 ± 1.390 |
| | 0.4 | 35649.01 ± 68744.12 | 139.37 ± 265.61 | 2.333 ± 0.204 |
| | 0.6 | 2197.63 ± 1945.48 | 10.09 ± 8.52 | 2.149 ± 0.152 |
| | 0.8 | 1131.36 ± 484.65 | 6.02 ± 2.31 | 1.861 ± 0.133 |
| **cPIM-1 with 5% Carbons** | 0.2 | 2967.24 ± 1206.40 | 12.69 ± 3.86 | 2.314 ± 0.398 |
| | 0.4 | 1688.12 ± 69.71 | 5.73 ± 1.17 | 3.008 ± 0.463 |
| | 0.6 | 904.89 ± 75.63 | 3.13 ± 0.24 | 2.897 ± 0.183 |
| | 0.8 | 768.06 ± 365.88 | 3.27 ± 1.79 | 2.409 ± 0.168 |
| **cPIM-1 with 2% Carbons** | 0.2 | 13016.84 ± 20854.24 | 61.07 ± 78.05 | 1.634 ± 0.496 |
| | 0.4 | 3374.32 ± 2202.50 | 12.76 ± 7.20 | 2.563 ± 0.199 |
| | 0.6 | 1645.38 ± 248.53 | 6.75 ± 1.28 | 2.456 ± 0.204 |
| | 0.8 | 1255.11 ± 299.01 | 5.77 ± 0.92 | 2.159 ± 0.180 |
| **cPIM-1 with 1% Carbons** | 0.2 | 3430.42 ± 1111.77 | 11.23 ± 4.19 | 3.141 ± 0.464 |
| | 0.4 | 7299.34 ± 10952.32 | 17.33 ± 23.97 | 3.692 ± 0.584 |
| | 0.6 | 1519.64 ± 444.84 | 5.06 ± 2.23 | 3.144 ± 0.560 |
| | 0.8 | 1133.96 ± 400.87 | 4.29 ± 0.73 | 2.593 ± 0.460 |

*Table 5.4: Permeability, diffusivity and solubility data of membranes of cPIM-1, cPIM-1 with 5% carbons w/w, cPIM-1 with 2% carbons w/w and cPIM-1 with 1% carbons w/w at different $H_2$ partial gas pressures.*

# 6. Improvements

An improved method was developed to obtain membranes without micro fractures and less fragile.

## *6.1.cPIM-1 based membrane with an improved preparation procedure*

The membrane preparation through the improved method involved the use of 562.5 mg of cPIM-1, 18 ml of NMP as solvent and glass fiber as support with a section of 4x5 cm. The procedure can be summarized in the following steps:

1. the glass fiber was weighed,
2. the cPIM-1 was solubilized in the solvent through sonication,
3. the solution obtained was sprayed on the glass fiber,
4. the impregnated support was placed on a glass petri and heated to 150 °C for few minutes,
5. the membrane was transferred to vacuum oven at 40 °C for 15-20 min,
6. steps 2, 3 and 4 were repeated for an optimal number of times,
7. the membrane was put under vacuum conditions at 100 °C (Buchi),
8. the glass fiber was weighed to calculate the amount of impregnated solution.

| | **Membrane of cPIM-1** |
|---|---|
| **Glass fiber** | 144.43 mg |
| **Glass fiber with solution** | 306.77 mg |

*Table 6.1: cPIM-1 based membrane quantities with the improved procedure.*

At the exit of Buchi, the membrane results completely dried and less fragile, as shown in Figure 6.1.

*Figure 6.1: Membranes of cPIM-1 realized on glass fiber.*

## *6.2.cPIM-1 with carbons-based membrane with an improved preparation procedure*

The preparation of membrane with the improved method required firstly the solubilization of cPIM-1 with NMP and carbons with NMP, that was realized separately by sonication to ensure a good dispersion of carbons. Subsequently, they were mixed into a single vial and additionally sonicated. The procedure is the same described in points 2, 3, 4, 5, 6, 7, 8 of section 3.1.7. All the interesting data are reported in the Tables 6.2 and 6.3.

| **Membrane** | **cPIM-1 (mg)** | **Solvent (ml)** | **Carbons (mg)** |
|---|---|---|---|
| 5% w/w | 750 | 24 | 39.5 |
| 2% w/w | 750 | 24 | 15.3 |
| 1% w/w | 750 | 24 | 7.6 |

*Table 6.2: cPIM-1 with carbons-based membrane quantities with the improved procedure.*

| | **Membrane of cPIM-1 with 5% carbons w/w** | **Membrane of cPIM-1 with 2% carbons w/w** | **Membrane of cPIM-1 with 1% carbons w/w** |
|---|---|---|---|
| **Glass fiber** | 112.98 mg | 115.37 mg | 109.31 mg |
| **Glass fiber with solution** | 371.62 mg | 267.81 mg | 256.43 mg |

*Table 6.3: Weight of glass fiber w/ and w/o solution.*

At the exit of Buchi, the membranes result completely dried and less fragile, as shown in Figure 6.2.

*Figure 6.2: Membranes of cPIM-1 with 5 % carbons (on the left), 2 % carbons (at the center), 1 % carbons (on the right) realized on glass fiber.*

# 7. Future perspectives

## *7.1.Flow cell*

The realization of membranes of cPIM-1 with different percentages of carbons obtained through the improved procedure, described in Chapter 6, offers the opportunity to investigate in a deeper way the membranes performance. In fact, it possible to test the membranes in a flow cell exposed to different fluxes of gases with the aim of determining more precise diffusivity values, compared to those obtained from the DVS instrument.

The flow cell is composed of two gas storage regions separated solely by the membrane positioned at the center across a 10 $cm^2$ area. This cell is subjected to diverse gas fluxes regulated by mass flows. By employing a gas chromatograph (μGC, Inficon Fusion®) with two columns (a 10m Rt-Molsieve 5A and an 8m Rt-Q-Bond) and micro thermal conductivity detectors, the signals of nitrogen, $N_2$, and carbon dioxide, $CO_2$, can be observed.

The experimental set-up is shown in Figure 7.1.

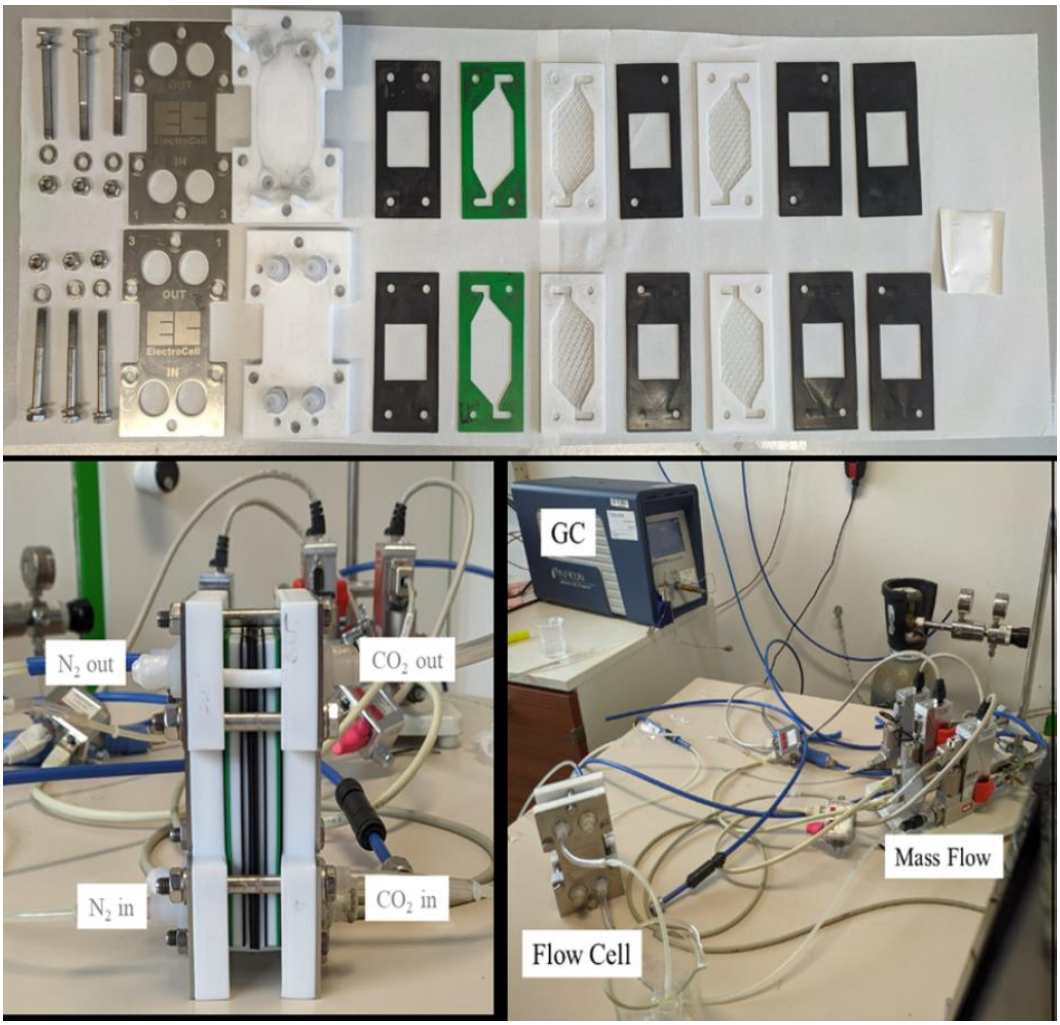


*Figure 7.1: Experimental set up including gas chromatograph, flow cell and mass flow.*

The $CO_2$ signal is monitored every four minutes through the gas chromatograph, GC. A series of rising values are obtained, up to a plateau value. The interpolation of the experimental points could be made through Origin, a data analysis software, using the following exponential decay function:

$$y = y_0 + A_1 \cdot e^{-\frac{x}{t_1}}$$

where:

$k = -\frac{x}{t_1}$ is the decay rate,

$y_0$ is the plateau value, which represents the maximum value of $CO_2$ crossing the membrane.

The parameter $y_0$ serves as an index of diffusivity, to which the mathematical model will subsequently be applied for deriving membrane diffusivity values. These values will consider the distinct pressures employed in the two methods used for assessing gas separation. The evaluation of the results obtained for cPIM-1 membranes with 5%, 2% and 1% of carbons will be performed.

# 8. Conclusions

The climate crisis is the greatest challenge facing our world. Right now, increased global average temperatures are having a profound effect on our climate and those effects will become more severe in the coming years.

Several countries are exploring strategies like carbon capture and storage (CCS) to reduce $CO_2$ emissions, that is the main component of greenhouse gas (GHG). [1]

This research is focused on the relatively novel capture concept of selective membranes used to separate certain components from a gas stream [9]. In particular, the main goal of this research is the development and assessment of Mixed Matrix Membranes (MMM) infused with Carbon-modified Polymers of Intrinsic Microporosity (PIMs) to enhance $CO_2$ separation efficiency.

The initial part of the study was dedicated to the synthesis of PIM-1, carboxylated PIM-1 and mesoporous carbons, together with the fabrication of membranes with varying carbon percentages, specifically 5 wt%, 2 wt% and 1 wt%. Several tests were performed to determine the best production procedure and solution to obtain flexible membranes without micro fractures, resulting with the use of NMP, as solvent, and LDPE, as support.

All membranes were characterized through structural (FT-IR), thermal (TGA and DSC), and morphological (FESEM) characterizations.

The efficiency of the membranes in gas separation technology is predominantly governed by the selectivity and permeability parameters. To assess these factors, adsorption-desorption measurements of pure $CO_2$, $CH_4$, $H_2$ and $N_2$ were conducted utilizing a Surface Measurement System Dynamic Vapor Sorption (DVS) instrument. The experiments were carried out at a consistent temperature of 40 °C with a gradual increase in pressure up to 0.8 bar. Consequently, solubility, permeability, and diffusion coefficients were determined for all samples.

Concluding this research, several key insights have emerged regarding the performance of different membranes in gas transport, particularly in relation to their permeability and solubility characteristics for various gases. These findings offer valuable implications for the field of membrane technology and its applications in gas separation and environmental management.

1. **Reliability and Predictability**: A notable observation is the consistency in permeability across different membranes for gases such as nitrogen and methane at various concentrations. This consistency underscores the reliability and predictability of these membranes in gas transport applications.
2. **Impact of Carbon Content**:
    - **Decreased Nitrogen Solubility**: An increase in carbon content within the membranes leads to decreased nitrogen solubility, particularly at 1 wt% and 2 wt% carbon. This reduction enhances the membranes' effectiveness in $CO_2$ separation.
    - **Reduced Methane Solubility**: Similarly, methane solubility decreases with an increase in carbon content, improving the membranes' separation characteristics.

- **Enhanced Carbon Dioxide Solubility**: Notably, $CO_2$ solubility increases with higher carbon content in the membranes, peaking at 5.0 wt% carbon. This enhancement is particularly significant for $CO_2$ transport and separation.

3. **Methodological Considerations**: It is important to note that the current methodologies for measuring permeability are less effective in extremely high permeability scenarios, like those observed with PIMs membranes. However, solubility measurements are consistently reliable, suggesting a need for more advanced measurement techniques in certain cases.
4. **Implications for Gas Separation**: The findings from this study highlight the potential of these membranes in selective gas separation. The differential impact of carbon content on various gases, especially the improved separation capabilities for $CO_2$, opens up avenues for industrial and environmental applications.
5. **Future Directions**: This research paves the way for further exploration and development in membrane technology. Understanding how factors like carbon content and membrane composition influence gas transport can guide the design of more efficient and targeted membrane systems. Such advancements could have significant implications in industries requiring robust gas separation solutions, contributing to environmental sustainability and efficient resource management.

In conclusion, this study has provided valuable insights into the capabilities and limitations of various membranes in gas transport, emphasizing the role of carbon content and highlighting the need for improved measurement techniques. These findings not only enhance our understanding of membrane technology but also offer practical solutions for real-world challenges in gas separation.

# 9. Acknowledgements

The research carried out in this thesis would not have been possible without the invaluable help of my supervisors who accompanied me in its development.

I would like to thank my supervisor Sergio Bocchini, for giving me the opportunity to work in research and development at the Italian Institute of Technology. Thank you for your professionalism, expertise and helpfulness.

Invaluable was the help of Carmela Astorino, who guided me every step of the way on this journey always with kindness, positivity and cheerfulness. It was a real pleasure to know you, to discover that we have some similar character aspects and, most of all, to be "your thesis student." Thank you, Mela.

I would like to thank Giuseppe Ferraro, who first welcomed me and reminded me that the main thing is to never lose focus. Thank you for generously sharing your knowledge and experience, and especially for helping me to believe more in myself. Thank you, Peppe.

Thank you, finally, to all the people who work in IIT. Each of you, even unknowingly, has enriched me not only professionally but also humanly.

It has been an unforgettable academic and life experience that I will always keep in my heart.

# 10.References

## *10.1. Bibliography*


[1] Sifat, N. S., & Haseli, Y. (2019). A critical review of $CO_2$ capture technologies and prospects for clean power generation. Energies, 12(21), 4143.

[2] Yadav, S., & Mondal, S. S. (2022). A review on the progress and prospects of oxy-fuel carbon capture and sequestration (CCS) technology. Fuel, 308, 122057.

[3] Leung, D. Y., Caramanna, G., & Maroto-Valer, M. M. (2014). An overview of current status of carbon dioxide capture and storage technologies. Renewable and sustainable energy reviews, 39, 426-443.

[4] Bui, M., Adjiman, C. S., Bardow, A., Anthony, E. J., Boston, A., Brown, S., ... & Mac Dowell, N. (2018). Carbon capture and storage (CCS): the way forward. Energy & Environmental Science, 11(5), 1062-1176.

[5] Alalaiwat, D., & Khan, E. (2023). Current status and future scenarios of carbon capture from power plants emission: a review. Reviews in Environmental Science and Bio/Technology, 22(3), 799-822.

[6] Gibbins, J., & Chalmers, H. (2008). Carbon capture and storage. Energy policy, 36(12), 4317-4322.

[7] Imteyaz, B., Qadir, S. A., & Tahir, F. (2021). Prospects of $CO_2$ utilization after carbon capture process. Fuel, 2, $N_2$.

[8] Mondal, M. K., Balsora, H. K., & Varshney, P. (2012). Progress and trends in $CO_2$ capture/separation technologies: A review. Energy, 46(1), 431-441.

[9] Olajire, A. A. (2010). $CO_2$ capture and separation technologies for end-of-pipe applications–A review. Energy, 35(6), 2610-2628.

[10] Bernardo, P., Drioli, E., & Golemme, G. (2009). Membrane gas separation: a review/state of the art. Industrial & engineering chemistry research, 48(10), 4638-4663.

[11] Sanders, D. F., Smith, Z. P., Guo, R., Robeson, L. M., McGrath, J. E., Paul, D. R., & Freeman, B. D. (2013). Energy-efficient polymeric gas separation membranes for a sustainable future: A review. Polymer, 54(18), 4729-4761.

[12] Han, Y., & Ho, W. W. (2021). Polymeric membranes for $CO_2$ separation and capture. Journal of Membrane Science, 628, 119244.

[13] Chung, T. S., Jiang, L. Y., Li, Y., & Kulprathipanja, S. (2007). Mixed matrix membranes (MMMs) comprising organic polymers with dispersed inorganic fillers for gas separation. Progress in polymer science, 32(4), 483-507.

[14] Mizrahi Rodriguez, K., Wu, A. X., Qian, Q., Han, G., Lin, S., Benedetti, F. M., ... & Smith, Z. P. (2020). Facile and time-efficient carboxylic acid functionalization of PIM-1: effect on molecular packing and gas separation performance. Macromolecules, 53(15), 6220-6234.

[15] McKeown, N. B. (2020). Polymers of intrinsic microporosity (PIMs). Polymer, 202, 122736.

[16] Jue, M. L., McKay, C. S., McCool, B. A., Finn, M. G., & Lively, R. P. (2015). Effect of Nonsolvent Treatments on the Microstructure of PIM-1. Macromolecules, 48(16), 5780-5790.

[17] McKeown, N. B., & Budd, P. M. (2006). Polymers of intrinsic microporosity (PIMs): organic materials for membrane separations, heterogeneous catalysis and hydrogen storage. Chemical Society Reviews, 35(8), 675-683.

[18] Tamaddondar, M., Foster, A. B., Carta, M., Gorgojo, P., McKeown, N. B., & Budd, P. M. (2020). Mitigation of physical aging with mixed matrix membranes based on cross-linked PIM-1 fillers and PIM-1. ACS applied materials & interfaces, 12(41), 46756-46766.

[19] Yong, W. F., Li, F. Y., Chung, T. S., & Tong, Y. W. (2014). Molecular interaction, gas transport properties and plasticization behavior of cPIM-1/Torlon blend membranes. Journal of Membrane Science, 462, 119-130.

[20] Budd, P. M., Elabas, E. S., Ghanem, B. S., Makhseed, S., McKeown, N. B., Msayib, K. J., ... & Wang, D. (2004). Solution-processed, organophilic membrane derived from a polymer of intrinsic microporosity. Advanced Materials, 16(5), 456-459.

[21] Santoso, B., Yanaranop, P., Kang, H., Leung, I. K., & Jin, J. (2017). A critical update on the synthesis of carboxylated polymers of intrinsic microporosity (C-PIMs). Macromolecules, 50(7), 3043-3050.

[22] Oschatz, M., & Antonietti, M. (2018). A search for selectivity to enable $CO_2$ capture with porous adsorbents. Energy & Environmental Science, 11(1), 57-70.

[23] Maruccia, E., Lourenço, M. A., Priamushko, T., Bartoli, M., Bocchini, S., Pirri, F. C., ... & Gerbaldi, C. (2022). Nanocast nitrogen-containing ordered mesoporous carbons from glucosamine for selective $CO_2$ capture. Materials Today Sustainability, 17, 100089.

[24] Deng, X., Chen, K., & Tüysüz, H. (2017). Protocol for the nanocasting method: preparation of ordered mesoporous metal oxides. Chemistry of Materials, 29(1), 40-52.

[25] Tomé, L. C., & Marrucho, I. M. (2016). Ionic liquid-based materials: A platform to design engineered CO 2 separation membranes. Chemical Society Reviews, 45(10), 2785-2824.

[26] Ramimoghadam, D., Gray, E. M., & Webb, C. J. (2016). Review of polymers of intrinsic microporosity for hydrogen storage applications. International Journal of Hydrogen Energy, 41(38), 16944-16965.

[27] McKeown, N. B. (2012). Polymers of intrinsic microporosity. International Scholarly Research Notices, 2012.

## *10.2. Sitography*

https://analyticalscience.wiley.com/do/10.1002/imaging.3333/

https://webbook.nist.gov/cgi/cbook.cgi?ID=C7664417&Units=SI&Type=IR-SPEC&Index=1#IR-SPEC

https://www.pianetachimica.it/

# 11.Appendix

## *11.1. Membranes preparation tests*

| Solvent | Support material | Conditions | Result |
|---|---|---|---|
| DMF | Nylon | Heating plate at 90 °C<br><br>Drying under vacuum |  |
| DMSO | Nylon | Heating plate with a temperature range between 60 °C and 100 °C<br><br>Drying under vacuum |  |
| NMP | Nylon | Heating plate at 125 °C<br><br>Drying under vacuum<br>150 mg of cPIM-1 and 2 ml of solvent |  |

*Table 11.1: cPIM-1 based membrane prepared on nylon as support.*

| Solvent | Support material | Conditions | Result |
|---|---|---|---|
| DMF | PTFE | Heating plate<br><br>Drying under vacuum |  |
| DMSO | PTFE | Heating plate<br><br>Drying under vacuum |  |
| NMP | PTFE | Heating plate<br><br>Drying under vacuum |  |

*Table 11.2: cPIM-1 based membrane prepared on PTFE as support.*

| Solvent | Support material | Conditions | Result |
|---|---|---|---|
| DMF | LDPE | Heating plate<br><br>Drying under vacuum |  |
| DMSO | LDPE | Heating plate<br><br>Drying under vacuum |  |
| NMP | LDPE | Heating plate with a temperature range between 60 °C and 70 °C<br><br>Drying under vacuum<br><br>Optimized quantities: 200 mg of cPIM-1 and 3 ml of solvent | 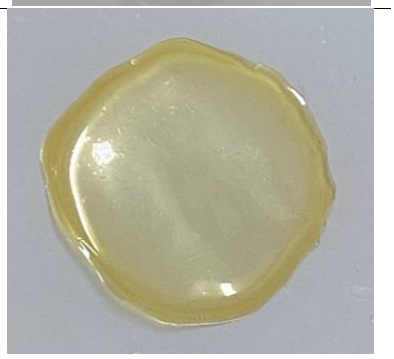 |

*Table 11.3: cPIM-1 based membrane prepared on LDPE as support.*